Electronic Supplementary Information for

Comparative bindings of lactones, lactide, and cyclic carbonates: experimental insights in the coordination step of polymerization

Kwanchanok Udomsasporn,[a] Setsiri Haesuwannakij,[a] Parichat Piromjitpong,[a] Phongnarin Chumsaeng,[a] and Khamphee Phomphrai*[a,b]

[a] Department of Materials Science and Engineering, School of Molecular Science and Engineering, Vidyasirimedhi Institute of Science and Technology (VISTEC), Wangchan, Rayong 21210, Thailand. Fax: +(66)-33-014-445; Tel: +(66)-33-014-151; Email: khamphee.p@vistec.ac.th.

[b] Research Network of NANOTEC-VISTEC on Nanotechnology for Energy, Vidyasirimedhi Institute of Science and Technology, Wangchan, Rayong 21210 Thailand

Table of Contents

1. General information

All operations were carried out under dry nitrogen atmosphere and used glovebox technique. Dichloromethane, n-hexane, and toluene were dried using a MB SPS 5 Mbraun solvent purification system packed with activated alumina and activated copper. Chemicals were purchased from commercial suppliers and used as received. L-Lactide was sublimed three times under vacuum before use. ε-Caprolactone (CL), δ-valerolactone (DVL), γ-butyrolactone (GBL), ethylene carbonate (EC), propylene carbonate (PC), propylene oxide (PO) and cyclohexene oxide (CHO) were dried over calcium hydride and distilled prior to use and stored in a glovebox at -30 °C. Benzene-d_6 was dried over 4 Å molecular sieves and stored under N_2.

^{1}H, $^{13}C\{^{1}H\}$, and $^{19}F\{^{1}H\}$ NMR spectra were recorded on a Bruker Ascend™ 600 and referenced to protio impurities of commercial C_6D_6 (residual internal C_6D_5H, $\delta = 7.16$ ppm) as internal standards. $^{19}F\{^{1}H\}$ NMR chemical shifts were referenced to protio impurities of deuterated solvent in the proton spectrum using the unified scale. X-ray crystallographic data were collected at 100, 110, 124, 127, 130, 140 K on a Bruker D8 venture using Photon II detector and IμS 3.0 Microfocus source, Mo K_α radiation ($\lambda = 0.71073$ Å). The frames were integrated with the *SAINT* software, and intensity data were corrected based on the intensities symmetry-related reflections measured at different angular setting (*SADABS*). The space group was determined with the *XPREP* software. The crystal structure was solved by intrinsic phasing method (*XT* program)[1] and refined by full-matrix least squares against F^2 using the program *XL* based on *ShelXle* engine.[2] The crystallographic images were processed by Ortep3 program.[3] Mass spectrometry was obtained by compact QTOF Bruker mass spectrometer. High resolution mass spectra were carried out using QtofControl analysis, atmospheric pressure compressed interface (APCI) mode. IR spectra were obtained with a ReactIR™ 15, equipped with a 6.3 mm AgX DiComp probe.

2. Synthesis and characterization

1:1 Reaction of $B(C_6F_5)_3$ and CL. ε-Caprolactone (4.6 mg, 0.040 mmol) and $B(C_6F_5)_3$ (21 mg, 0.040 mmol) were mixed in C_6D_6 in J-young NMR tube at room temperature. ^{1}H NMR (600 MHz, C_6D_6, 30 °C): δ 2.97 (t, 2H, J = 4.1 Hz, OCH_2), 1.67 (m, 2H, C(O)CH_2), 0.73 (m, 2H, J = 5.3 Hz, C(O)CH$_2$CH_2), 0.53 (m, 4H, CH_2). ^{13}C{^{1}H} NMR (150 MHz, C_6D_6, 30 °C): δ 189.06 (*C*=O), 149.17, 147.57, 141.34, 139.68, 138.39, 136.77 (m, C_6F_5), 75.76 (O*C*H$_2$), 33.79 (C(O)*C*H$_2$), 27.36, 26.87 (*C*H$_2$), 20.61 (C(O)CH$_2$*C*H$_2$). ^{19}F{^{1}H} NMR (565 MHz, C_6D_6, 30 °C): δ -134.76 (d, J = 22.8 Hz, *o*-F), -156.92 (t, J = 19.8 Hz, *p*-F), -163.99 (t, J = 18.7 Hz, *m*-F).

Crystal data for $B(C_6F_5)_3$·CL. The 1:1 mixture of **1** and CL was recrystallized by slow evaporation of toluene solution at -30 °C for several days to give colorless crystals. $C_{24}H_{10}BF_{15}O_2$, M_r = 626.13, triclinic, space group P -1, a = 10.3019(6) Å, b = 11.4706(7) Å, c = 11.9410(7) Å, α = 92.148(2)°, β = 103.691(2)°, γ = 107.901(2)°, V = 1295.29(13) Å^3, Z = 2, λ = 0.71073 Å, μ = 0.174 mm^{-1}, T = 110 K, 59809 reflections measured, 7961 independent reflections, R_{int} = 0.0306, R_1 = 0.0381 (obs. data), wR(F^2) = 0.1046 (obs. data), GOF = 1.032, CCDC 1995497.

1:1 Reaction of $B(C_6F_5)_3$ and DVL. δ-Valerolactone (4.0 mg, 0.040 mmol) and $B(C_6F_5)_3$ (21 mg, 0.040 mmol) were mixed in C_6D_6 in J-young NMR tube at room temperature. ^{1}H NMR (600 MHz, C_6D_6, 30 °C): δ 2.94 (t, 2H, J = 5.7 Hz, OCH_2), 1.62 (t, 2H, J = 6.8 Hz, C(O)CH_2), 0.49–0.25 (m, 4H, CH_2). ^{13}C{^{1}H} NMR (150 MHz, C_6D_6, 30 °C): δ 149.18, 147.58, 141.34, 139.69, 138.41, 136.77 (m, C_6F_5), 75.23 (O*C*H$_2$), 28.61 (*C*(O)CH$_2$), 20.34, 16.09 (*C*H$_2$) (*C*=O is not seen at room temperature due to equilibrium). ^{19}F{^{1}H} NMR (565 MHz, C_6D_6, 30 °C): δ -135.07 (d, J = 23.0 Hz, *o*-F), -156.95 (t, J = 20.8 Hz, *p*-F), -163.96 (t, J = 22.3 Hz, *m*-F).

Crystal data for $B(C_6F_5)_3$·DVL. The 1:1 mixture of **1** and DVL was recrystallized by layering hexanes on top of CH_2Cl_2 solution for several days at -30 °C to give colorless crystals. $C_{23}H_8BF_{15}O_2$, M_r = 612.10, monoclinic, space group C 1 2/c 1, a = 29.422(4) Å, b = 10.4028(13) Å, c = 15.1204(19) Å, α = 90°, β = 107.219(4)°, γ = 90°, V = 4420.5(10) Å^3, Z = 8, λ = 0.71073 Å, μ = 0.202 mm^{-1}, T = 130.(2) K, 78313 reflections measured, 4222 independent reflections, R_{int} = 0.0347, R_1 = 0.0323 (obs. data), wR(F^2) = 0.0777 (obs. data), GOF = 1.083, CCDC 1995504.

1:1 Reaction of $B(C_6F_5)_3$ and GBL. γ-Butyrolactone (3.4 mg, 0.040 mmol) and $B(C_6F_5)_3$ (21 mg, 0.040 mmol) were mixed in C_6D_6 in J-young NMR tube at room temperature. ^{1}H NMR (600 MHz, C_6D_6, 30 °C): δ 3.05 (t, 2H, J = 7.4 Hz, OCH_2), 1.59 (t, 2H, J = 8.3 Hz, C(O)CH_2), 0.58 (m, 2H, J = 7.9, 7.5 Hz, CH_2). ^{13}C{^{1}H} NMR (150 MHz, C_6D_6, 30 °C): δ 190.64 (*C*=O), 149.25, 147.66, 141.57, 139.91, 138.45, 136.83 (m, C_6F_5), 77.85 (O*C*H$_2$), 30.67 (C(O)*C*H$_2$), 20.08(*C*H$_2$). ^{19}F{^{1}H} NMR (565 MHz, C_6D_6, 30 °C): δ -134.96 (d, J = 23.1 Hz, *o*-F), -156.26 (t, J = 21.0 Hz, *p*-F), -163.68 (t, J = 22.5 Hz, *m*-F).

Crystal data for $B(C_6F_5)_3$·GBL. The 1:1 mixture of **1** and GBL was recrystallized by slow evaporation of benzene solution at room temperature for several days to give colorless crystals. $C_{22}H_6BF_{15}O_2$, M_r = 598.08, orthorhombic, space group P c a 2$_1$, a = 14.8191(9) Å, b = 13.9430(10) Å, c = 20.8344(15) Å, α = 90°, β = 90°, γ = 90°, V = 4304.9(5) Å^3, Z = 8, λ = 0.71073 Å, μ = 0.205 mm^{-1}, T = 100 K, 106403 reflections measured, 8858 independent reflections, R_{int} = 0.0712, R_1 = 0.0529 (obs. data), wR(F^2) = 0.1146 (obs. data), GOF = 1.050, CCDC 1995501.

1:1 Reaction of $B(C_6F_5)_3$ and LA. L-Lactide (5.8 mg, 0.040 mmol) and $B(C_6F_5)_3$ (21 mg, 0.040 mmol) were mixed in C_6D_6 in J-young NMR tube at room temperature. ^{1}H NMR (600 MHz, C_6D_6, 30 °C): δ 3.61 (q, 1H, J = 6.7 Hz, C*H*CH$_3$), 0.97 (d, 3H, J = 6.7 Hz, CHC*H*$_3$). ^{13}C{^{1}H} NMR (150 MHz, C_6D_6, 30 °C): δ 170.44 (*C*=O), 149.09, 147.48, 142.37, 140.86, 138.48, 136.84 (m, C_6F_5), 74.35 (*C*HCH$_3$), 14.89 (CH*C*H$_3$). ^{19}F{^{1}H} NMR (565 MHz, C_6D_6, 30 °C): δ -133.60 (d, J = 22.8 Hz, *o*-F), -151.96 (s, *p*-F), -162.41 (t, J = 20.6 Hz, *m*-F).

Crystal data for $B(C_6F_5)_3$·LA. The 1:1 mixture of **1** and LA was recrystallized by layering hexanes on top of CH_2Cl_2 solution for several days at -30 °C to give colorless crystals. $C_{42}H_8B_2F_{30}O_4$, M_r = 1168.10, orthorhombic, space group P 2$_1$ 2$_1$ 2$_1$, a = 14.4480(8) Å, b = 14.6266(9) Å, c = 18.8637(13) Å, α = 90°, β = 90°, γ = 90°, V = 3986.4(4) Å^3, Z = 4, λ = 0.71073 Å, μ = 0.218 mm^{-1}, T = 100 K, 67547 reflections measured, 12232 independent reflections, R_{int} = 0.0705, R_1 = 0.0417 (obs. data), wR(F^2) = 0.0999 (obs. data), GOF = 1.021, CCDC 1995502.

1:1 Reaction of $B(C_6F_5)_3$ and EC. Ethylene carbonate (3.5 mg, 0.040 mmol) and $B(C_6F_5)_3$ (21 mg, 0.040 mmol) were mixed in C_6D_6 in J-young NMR tube at room temperature. ^{1}H NMR (600 MHz, C_6D_6, 30 °C): δ 2.74 (s, 4H, CH_2). ^{13}C{^{1}H} NMR (150 MHz, C_6D_6, 30 °C): δ 163.2 (*C*=O), 149.31, 147.72, 142.13, 140.46, 138.47, 136.83 (m, C_6F_5), 68.45 (*C*H$_2$).

$^{19}F\{^{1}H\}$ NMR (565 MHz, C_6D_6, 30 °C): δ -134.55 (d, J = 22.9 Hz, *o*-F), -155.08 (s, *p*-F), -163.37 (m, *m*-F).

Crystal data for $B(C_6F_5)_3$·EC. The 1:1 mixture of **1** and EC was recrystallized by layering hexanes on top of CH_2Cl_2 solution for several days at room temperature to give colorless crystals. $C_{42}H_8B_2F_{30}O_6$, M_r = 1200.10, orthorhombic, space group P c a 2_1, a = 14.9675(8) Å, b = 13.4729(7) Å, c = 20.6890(10) Å, α = 90°, β = 90°, γ = 90°, V = 4172.1(4) Å^3, Z = 4, λ = 0.71073 Å, μ = 0.215 mm^{-1}, T = 124.(2) K, 106695 reflections measured, 10807 independent reflections, R_{int} = 0.0447, R_1 = 0.0357 (obs. data), wR(F^2) = 0.0724 (obs. data), GOF = 1.043, CCDC 1995505.

1:1 Reaction of $B(C_6F_5)_3$ and PC. Propylene carbonate (4.1 mg, 0.040 mmol) and $B(C_6F_5)_3$ (21 mg, 0.040 mmol) were mixed in C_6D_6 in J-young NMR tube at room temperature. ^{1}H NMR (600 MHz, C_6D_6, 30 °C): δ 3.34 (m, 1H, J = 6.7 Hz, C*H*), 3.05-2.38 (dt, 2H, CH_2), 0.09 (d, 3H, J = 6.4 Hz, CH_3). $^{13}C\{^{1}H\}$ NMR (150 MHz, C_6D_6, 30 °C): δ 163.01 (*C*=O), 149.29, 147.70, 143.03, 141.34, 138.50, 136.85 (m, C_6F_5), 80.38 (*C*H_2), 73.69 (*C*H), 17.39 (*C*H_3). $^{19}F\{^{1}H\}$ NMR (565 MHz, C_6D_6, 30 °C): δ -134.84 (d, J = 22.7 Hz, *o*-F), -156.17 (t, J = 20.7 Hz, *p*-F), -163.77 (m, *m*-F).

Crystal data for $B(C_6F_5)_3$·PC. The 1:1 mixture of **1** and PC was recrystallized by layering hexanes on top of CH_2Cl_2 solution for several days at -30 °C to give colorless crystals. $C_{22}H_6BF_{15}O_3$, M_r = 614.08, triclinic, space group P -1, a = 10.3038(6) Å, b = 12.6157(8) Å, c = 17.6372(12) Å, α = 96.426(3)°, β = 92.793(3)°, γ = 103.676(2)°, V = 2206.9(2) Å^3, Z = 4, λ = 0.71073 Å, μ = 0.205 mm^{-1}, T = 127 K, 37308 reflections measured, 8364 independent reflections, R_{int} = 0.0432, R_1 = 0.0444 (obs. data), wR(F^2) = 0.0998 (obs. data), GOF = 1.087, CCDC 1995503.

1:1 Reaction of $B(C_6F_5)_3$ and PO. Propylene oxide (2.3 mg, 0.040 mmol) and $B(C_6F_5)_3$ (21 mg, 0.040 mmol) were mixed in C_6D_6 in J-young NMR tube at room temperature. The hydride shift reaction occurred within a few minutes. ^{1}H NMR (600 MHz, C_6D_6, 30 °C): δ 8.23 (s, 1H, C*H*O), 1.58 (q, 2H, J = 6.9 Hz, CH_2), 0.46 (t, 3H, J = 6.8 Hz, CH_3). $^{13}C\{^{1}H\}$ NMR (150 MHz, C_6D_6, 30 °C): δ 149.20, 147.59, 142.30, 140.55, 138.52, 136.97(m, C_6F_5), 36.49 (*C*H_2), 5.13 (*C*H_3). $^{19}F\{^{1}H\}$ NMR (565 MHz, C_6D_6, 30 °C): δ -134.11 (d, J = 23.2 Hz, *o*-F), -153.68 (s, *p*-F), -162.45 (s, *m*-F).

Crystal data for $CH_3CH_2CHO{\cdot}B(C_6F_5)_3$. The product was recrystallized by layering hexanes on top of CH_2Cl_2 solution for several days at -30 ˚C to give colorless crystals. $C_{21}H_6BF_{15}O$, M_r = 570.07, monoclinic, space group P 1 2_1/n 1, a = 11.5139(8) Å, b = 9.2262(6) Å, c = 19.1731(13) Å, α = 90°, β = 90.084(3)°, γ = 90°, V = 2036.7(2) Å^3, Z = 4, λ = 0.71073 Å, μ = 0.208 mm^{-1}, T = 140.(2) K, 56448 reflections measured, 4461 independent reflections, R_{int} = 0.0779, R_1 = 0.0541 (obs. data), wR(F^2) = 0.1310 (obs. data), GOF = 1.021, CCDC 1995506.

1:1 Reaction of $B(C_6F_5)_3$ and CHO. Cyclohexene oxide (3.9 mg, 0.040 mmol) and $B(C_6F_5)_3$ (21 mg, 0.040 mmol) were mixed in C_6D_6 in J-young NMR tube at room temperature. Oligo(cyclohexene oxide) was obtained within a few minutes. ^{1}H NMR (600 MHz, C_6D_6, 30 °C): *δ* 3.79-3.57 (br), 2.12 (br), 1.76-1.33 (br). APCI-MS (m/z) 99.06, 197.13, 295.19, 393.26, 491.32, 589.39 for $(CHO)_n + H^+$ (n = 1-6); 215.14, 313.20, 411.27, 509.33, 607.40, 705.47, 803.53 for $H(CHO)_nOH + H^+$ (n = 2-8).

References

1. Sheldrick, G. M., SHELXT–Integrated space-group and crystal-structure determination. *Acta Crystallogr. Sect. A: Found. Adv.* **2015,** *71*, 3-8.

2. Sheldrick, G. M., Crystal structure refinement with SHELXL. *Acta Crystallogr. Sec. C: Struct. Chem.* **2015,** *71*, 3-8.

3. Farrugia, L. J., WinGX and ORTEP for Windows: an update. *J. Appl. Crystallogr.* **2012,** *45*, 849-854.

3. X-ray crystallography

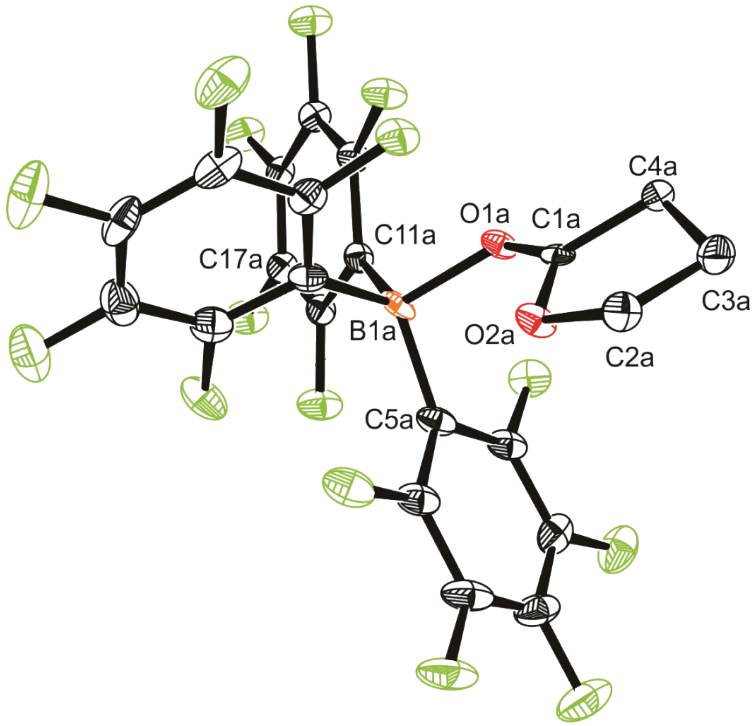

Figure S1 X-ray crystal structure of $B(C_6F_5)_3 \cdot$GBL adduct with thermal ellipsoids drawn at 50% probability level. Hydrogen atoms are omitted for clarity. Selected bond distances (Å) and angles (°): B1a–O1a 1.581(6), C1a–O1a 1.252(5), C1a–O2a 1.293(5), B1a–O1a–C1a 124.9(3), O1a–C1a–O2a 122.0(4), O2a–C1a–C4a 113.7(4), O1a–C1a–C4a 124.2(4), O1a–B1a–C11a 103.9(3), O1a–B1a–C17a 110.8(4), O1a–B1a–C5a 102.4(4).

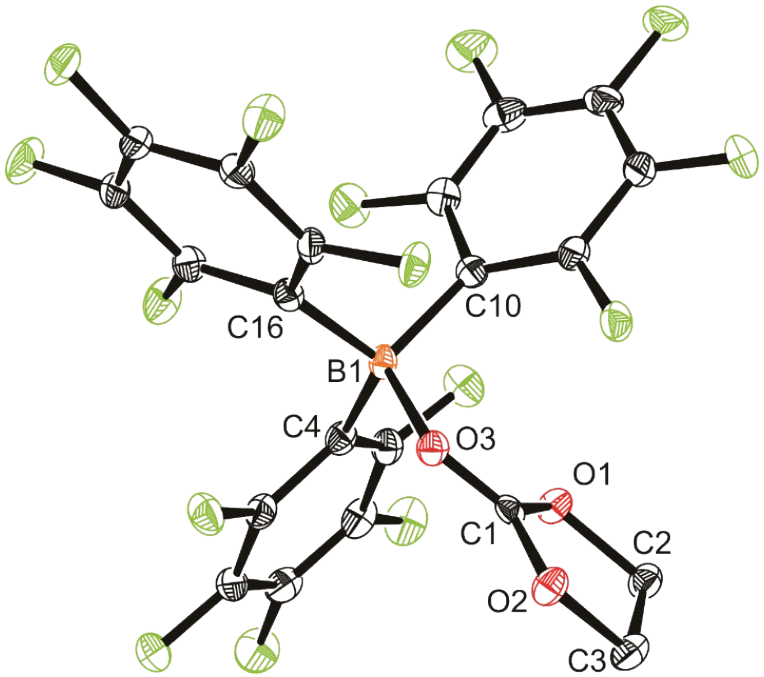

Figure S2 X-ray crystal structure of $B(C_6F_5)_3 \cdot EC$ adduct with thermal ellipsoids drawn at 50% probability level. Hydrogen atoms are omitted for clarity. Selected bond distances (Å) and angles (°): B1–O3 1.591(4), C1–O3 1.242(3), C1–O1 1.302(3), C1–O2 1.301(3), B1–O3–C1 122.0(2), O3–C1–O1 123.7(2), O3–C1–O2 120.7(2), O1–C1–O2 115.6(2), O3–B1–C4 102.7(2), O3–B1–C10 110.7(2), O3–B1–C16 104.6(2).

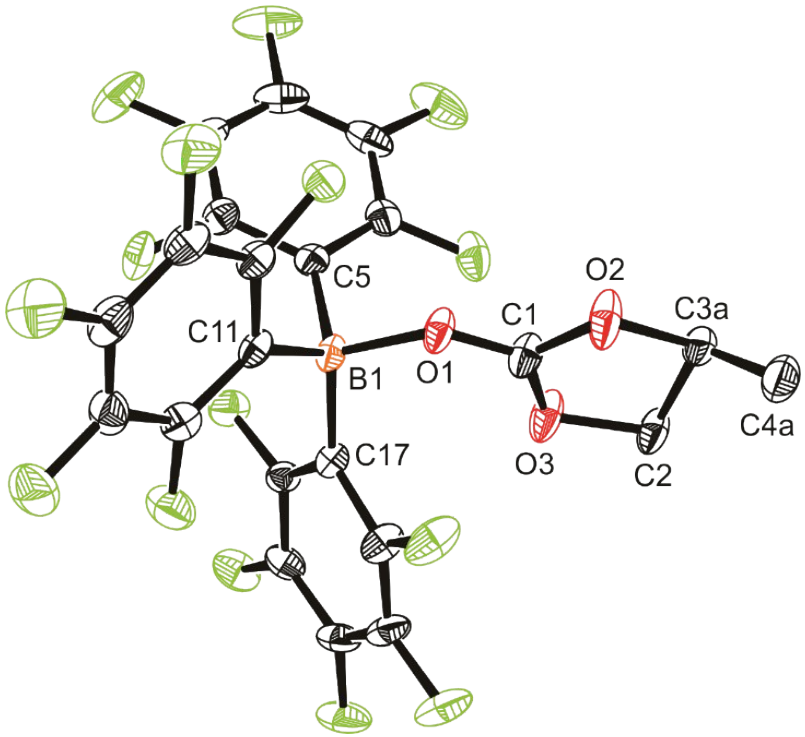

Figure S3 X-ray crystal structure of $B(C_6F_5)_3 \cdot PC$ adduct with thermal ellipsoids drawn at 50% probability level. Hydrogen atoms are omitted for clarity. Selected bond distances (Å) and angles (°): B1–O1 1.589(3), C1–O1 1.232(3), C1–O2 1.296(3), C1–O3 1.306(3), B1–O1–C1 133.4(2), O1–C1–O2 119.9(2), O1–C1–O3 125.3(2), O2–C1–O3 114.9(2), O1–B1–C5 104.2(2), O1–B1–C11 100.9(2), O1–B1–C17 110.5(2).

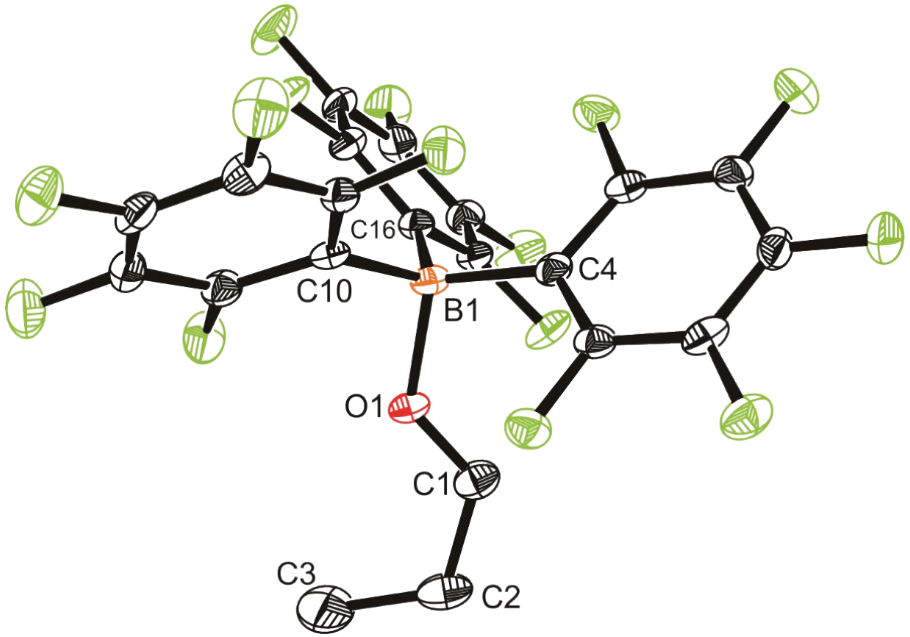

Figure S4 X-ray crystal structure of $B(C_6F_5)_3 \cdot OCHCH_2CH_3$ adduct with thermal ellipsoids drawn at 50% probability level. Hydrogen atoms are omitted for clarity. Selected bond distances (Å) and angles (°): B1–O1 1.626(3), C1–O1 1.241(3), B1–O1–C1 128.4(2), O1–B1–C4 107.7(2), O1–B1–C10 101.1(2), O1–B1–C16 103.3(2).

4. NMR and IR spectroscopy

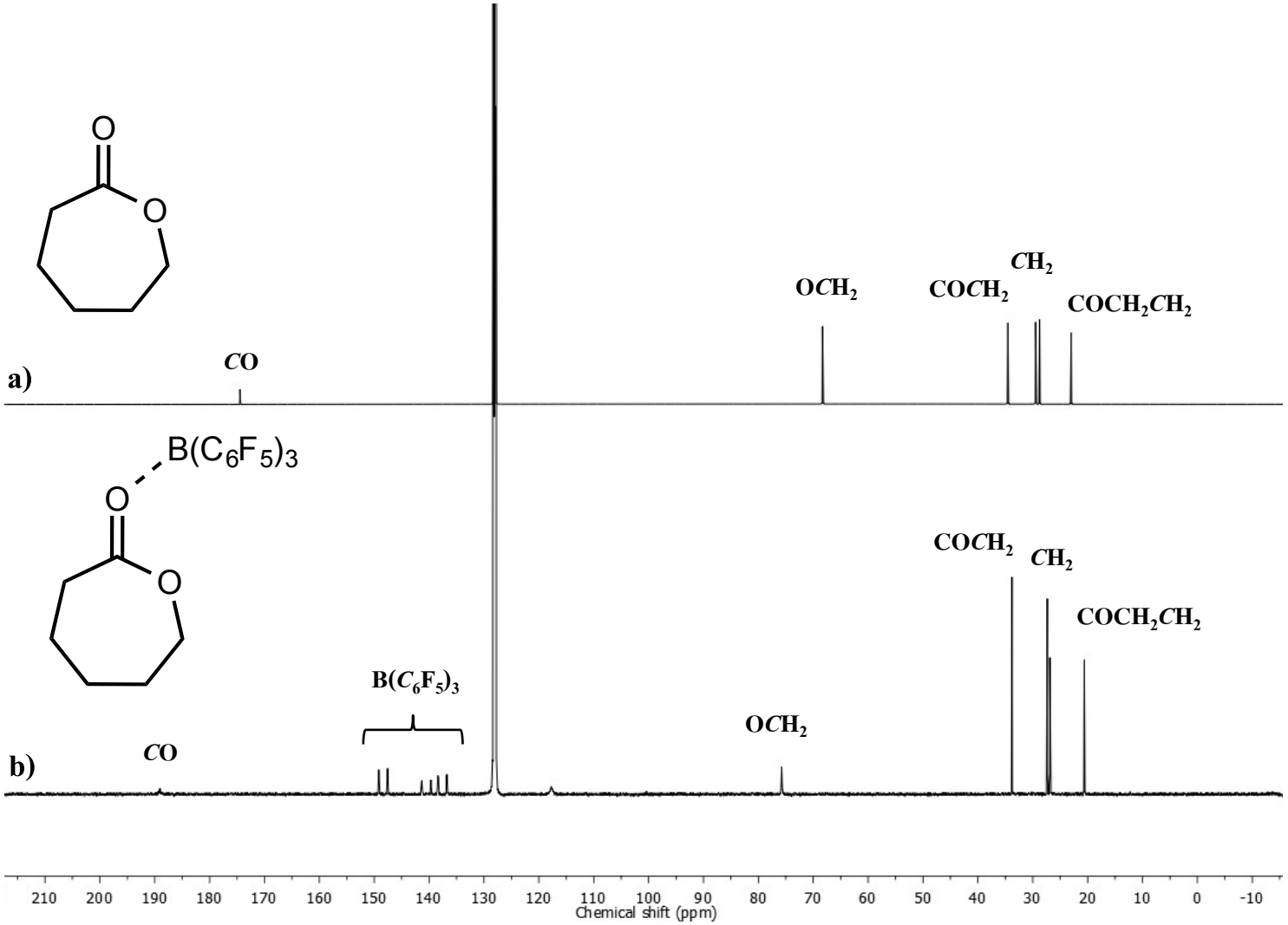

Figure S5 $^{13}C\{^{1}H\}$ NMR spectra (150 MHz, C_6D_6, 30 °C) of a) CL monomer and b) $B(C_6F_5)_3$·CL adduct

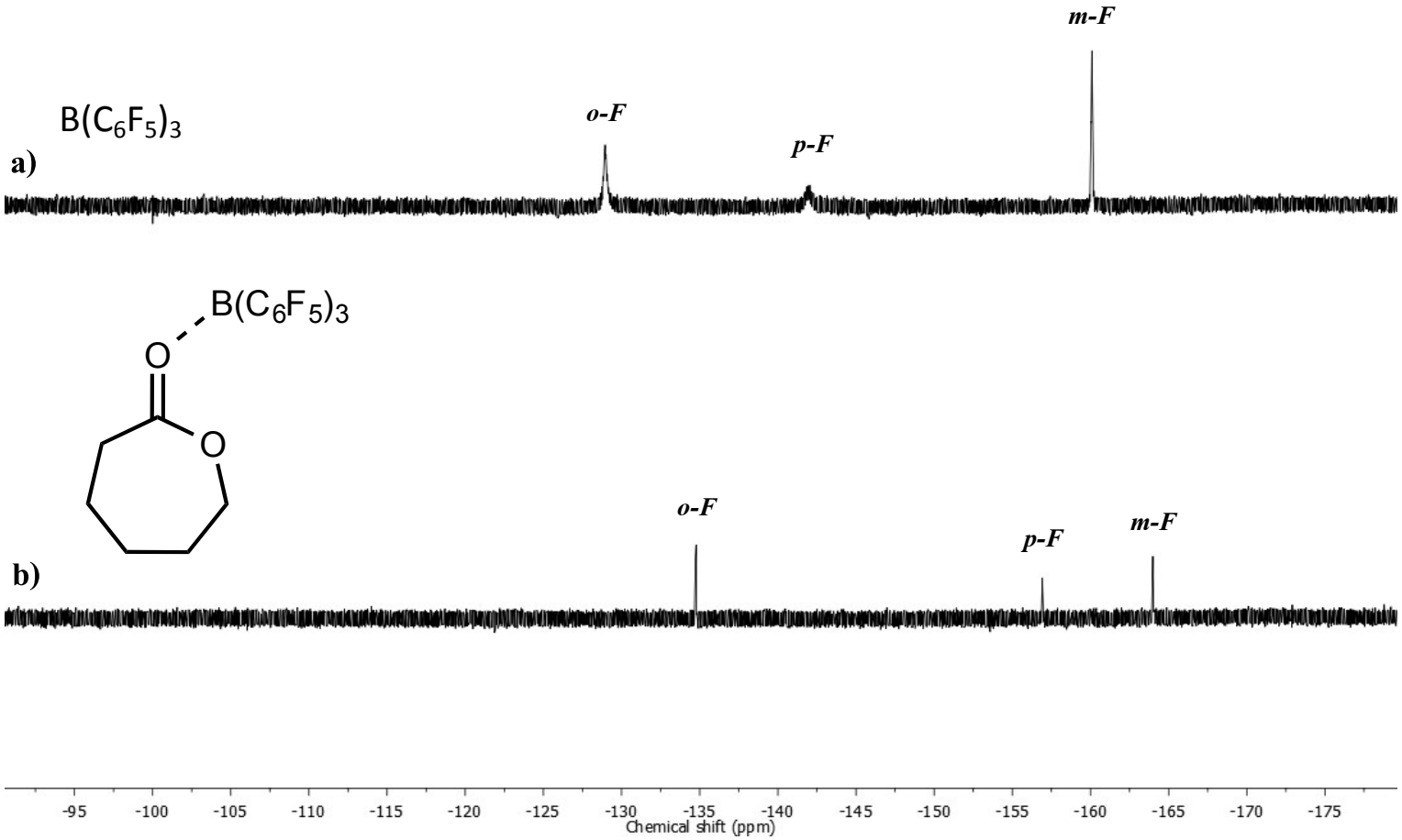

Figure S6 $^{19}F\{^{1}H\}$ NMR spectra (565 MHz, C_6D_6, 30 °C) of a) $B(C_6F_5)_3$ and b) $B(C_6F_5)_3$·CL adduct.

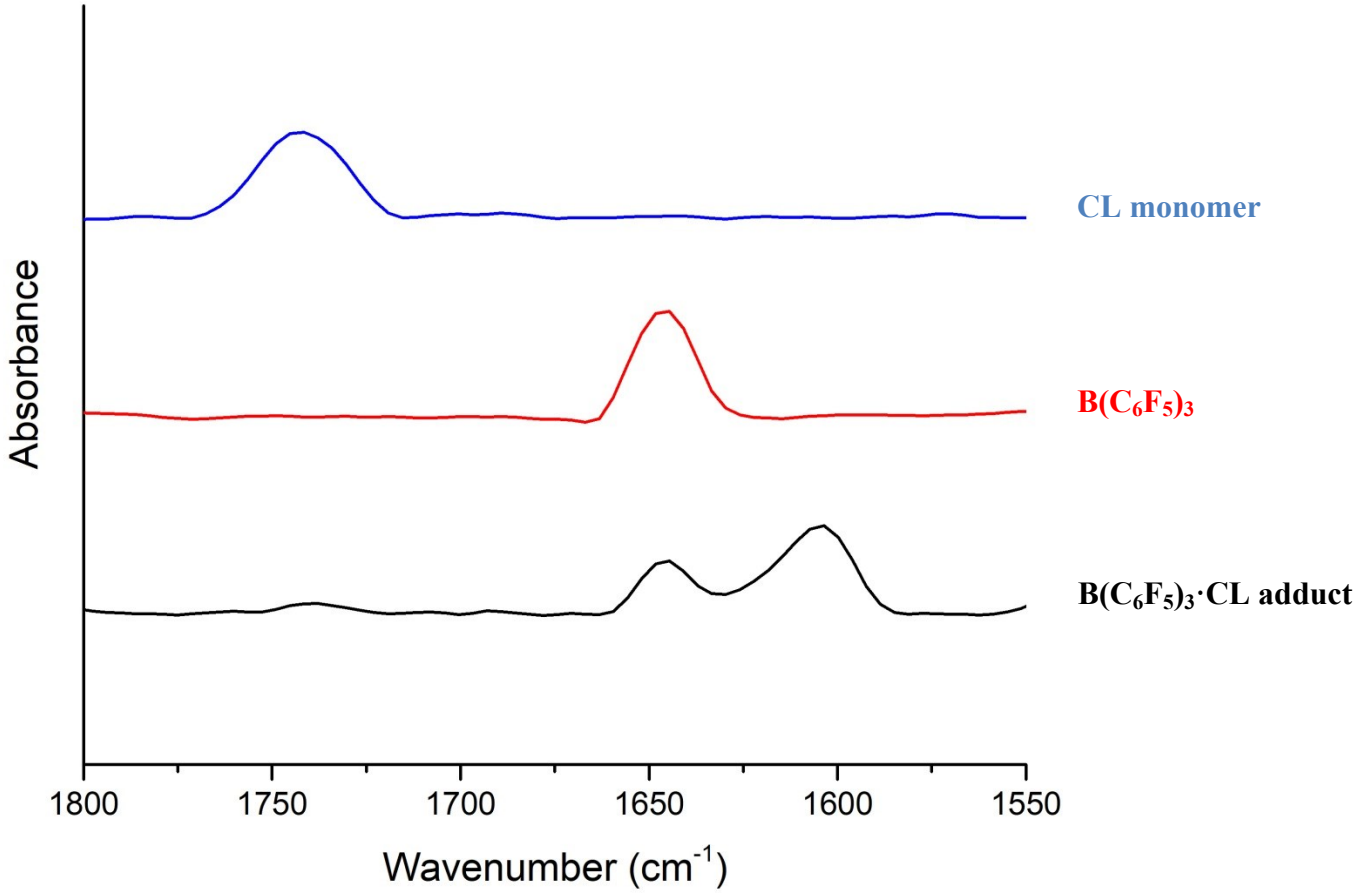

Figure S7 Selected IR spectra of $B(C_6F_5)_3$·CL adduct (black line), $B(C_6F_5)_3$ (red line), and CL monomer (blue line) in the region of 1800 – 1550 cm^{-1}. The relative intensities are normalized and thus are directly comparable.

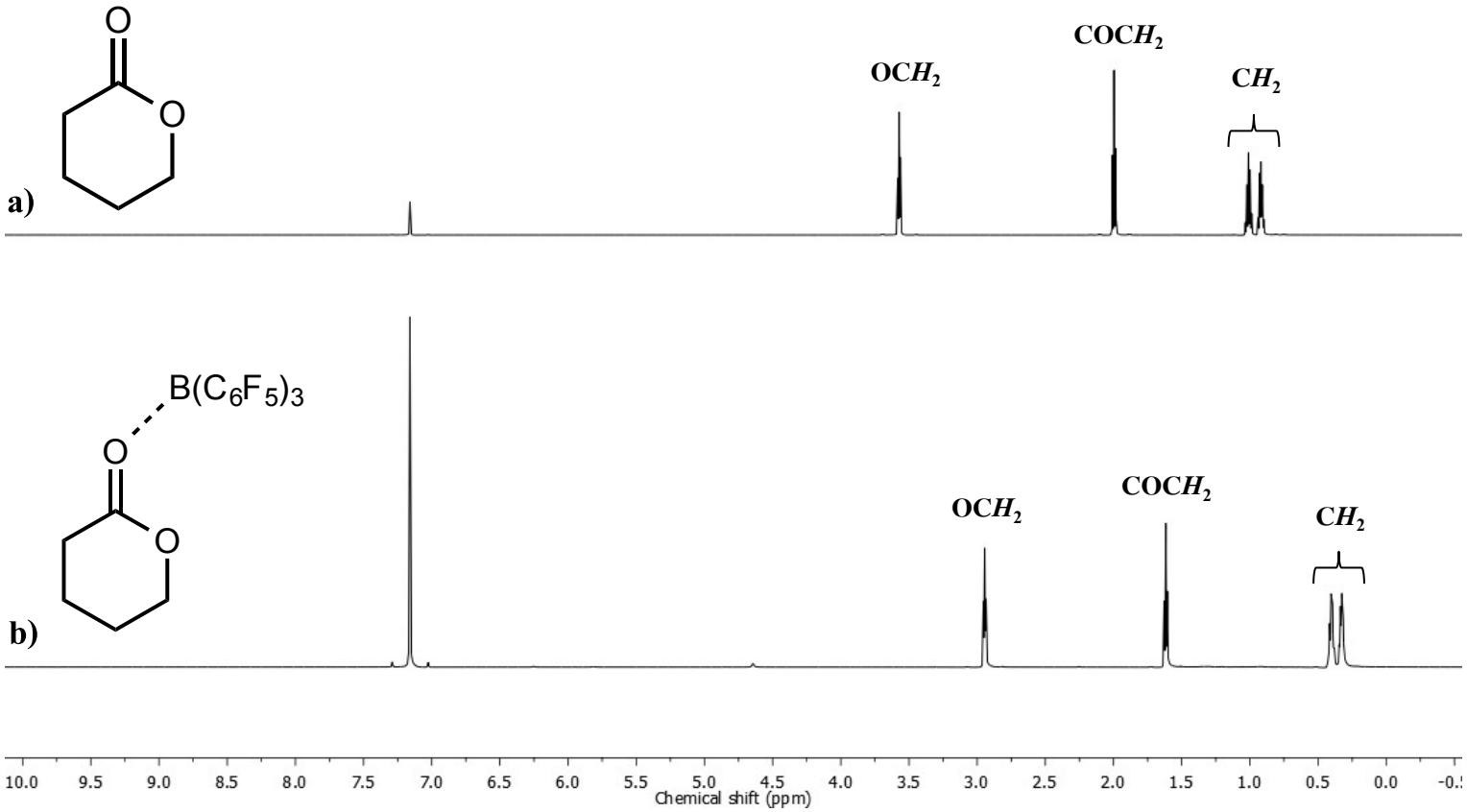

Figure S8 ^{1}H NMR spectra (600 MHz, C_6D_6, 30 °C) of a) DVL monomer and b) $B(C_6F_5)_3$·DVL adduct.

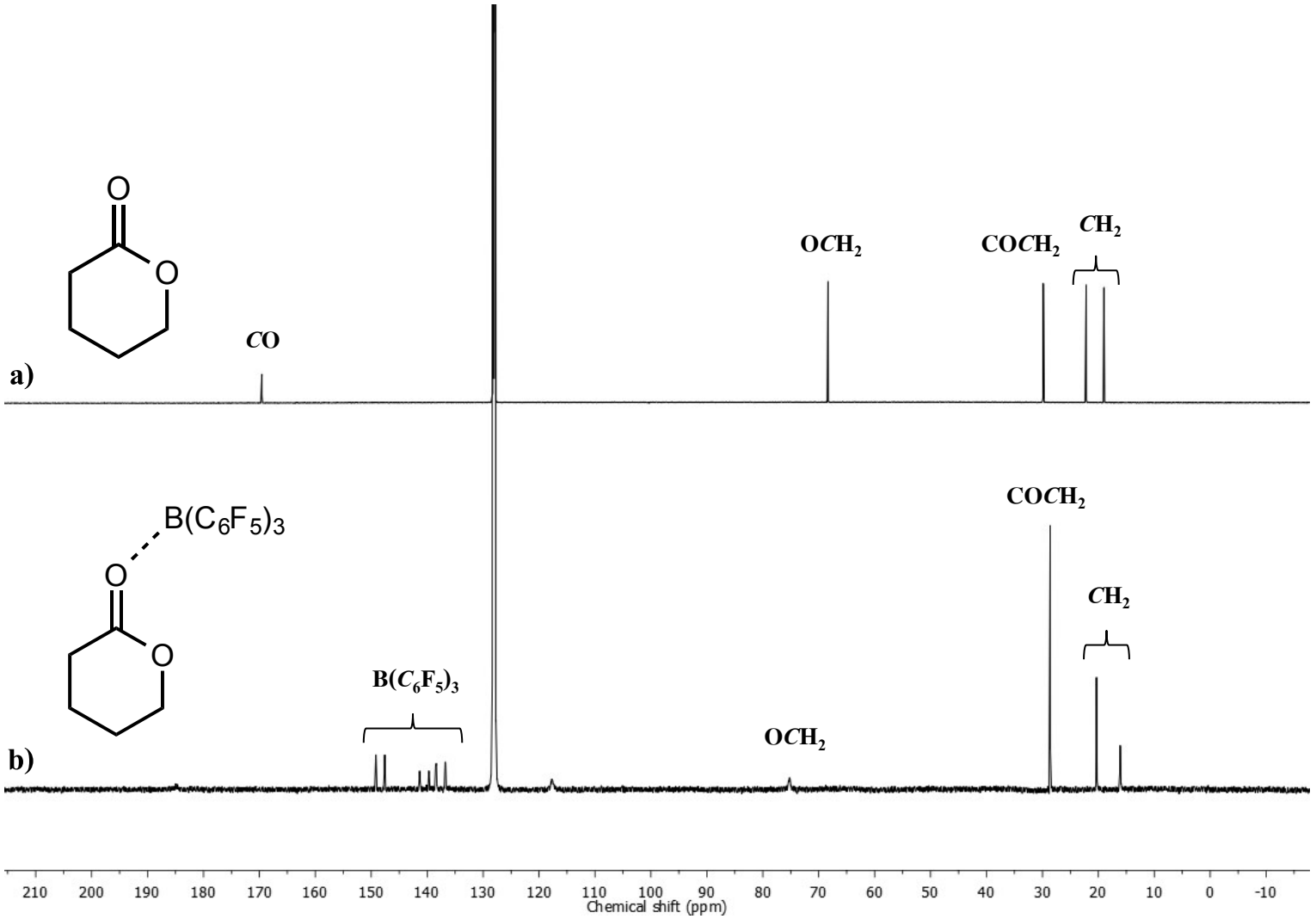

Figure S9 $^{13}C\{^{1}H\}$ NMR spectra (150 MHz, C_6D_6, 30 °C) of a) DVL monomer and b) $B(C_6F_5)_3$·DVL adduct.

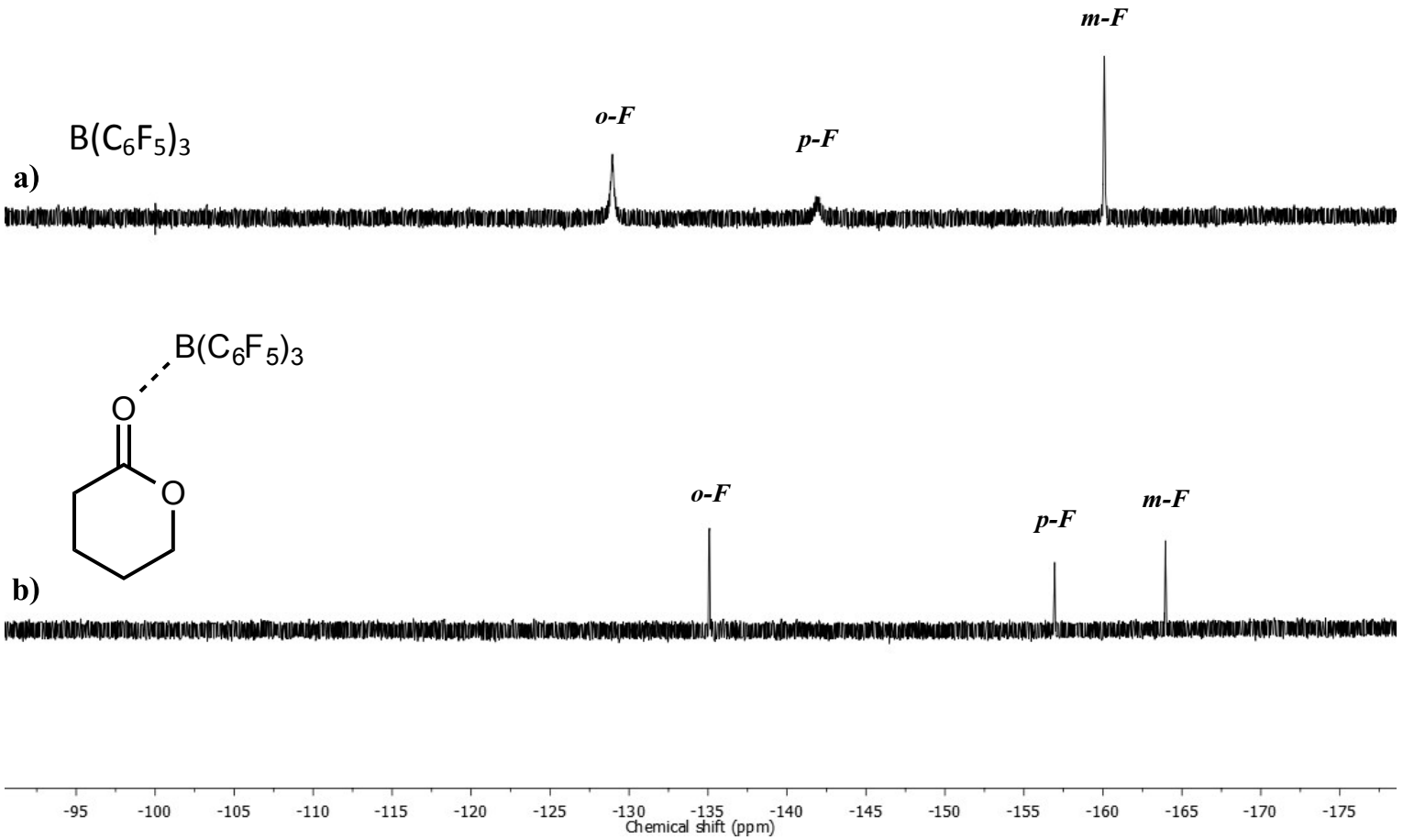

Figure S10 $^{19}F\{^{1}H\}$ NMR spectra (565 MHz, C_6D_6, 30 °C) of a) $B(C_6F_5)_3$ and b) $B(C_6F_5)_3$·DVL adduct.

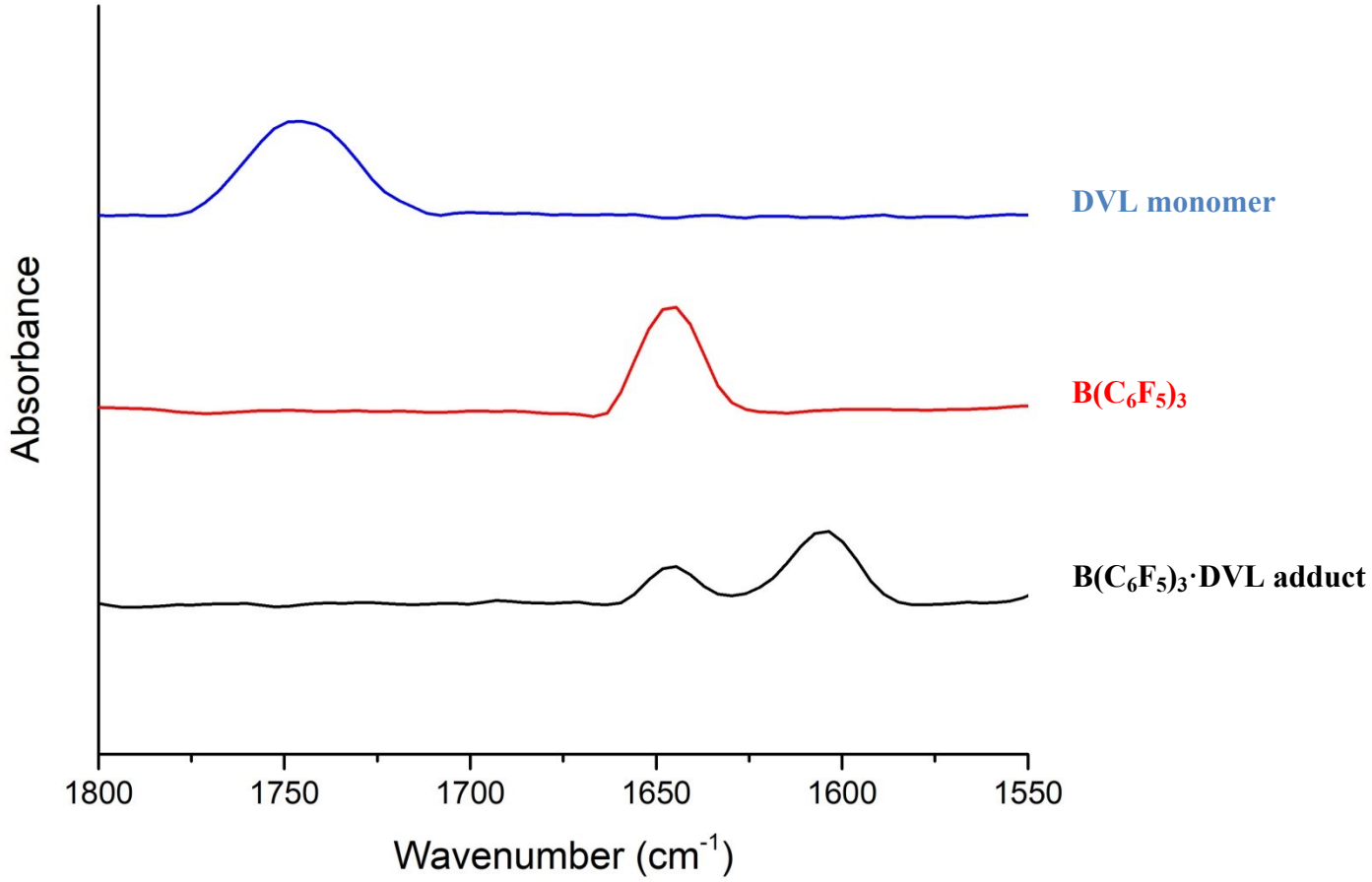

Figure S11 Selected IR spectra of $B(C_6F_5)_3$·DVL adduct (black line), $B(C_6F_5)_3$ (red line), and DVL monomer (blue line) in the region of 1800 – 1550 cm^{-1}. The relative intensities are normalized and thus are directly comparable.

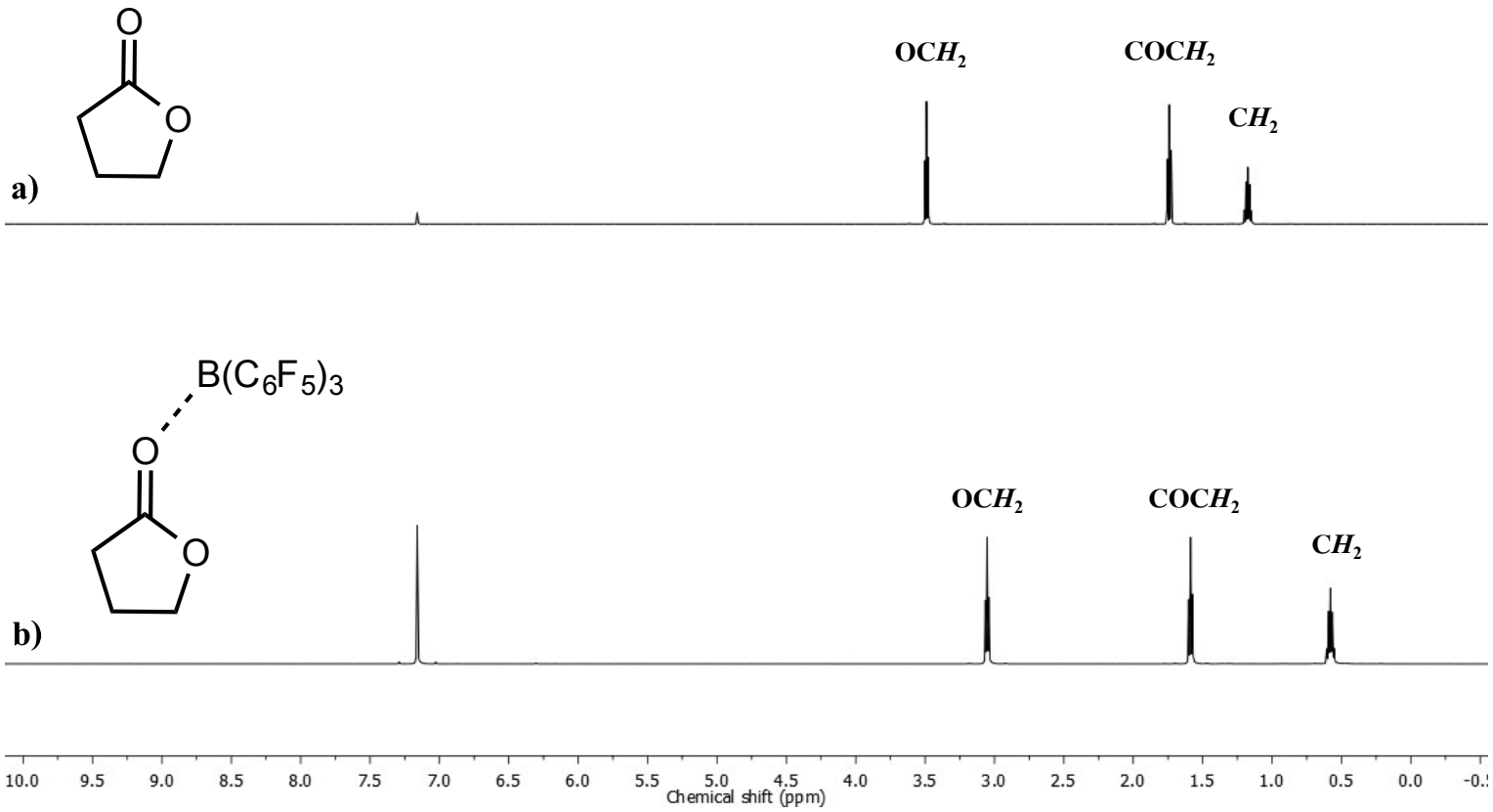

Figure S12 ^{1}H NMR spectra (600 MHz, C_6D_6, 30 °C) of a) GBL monomer and b) $B(C_6F_5)_3$·GBL adduct.

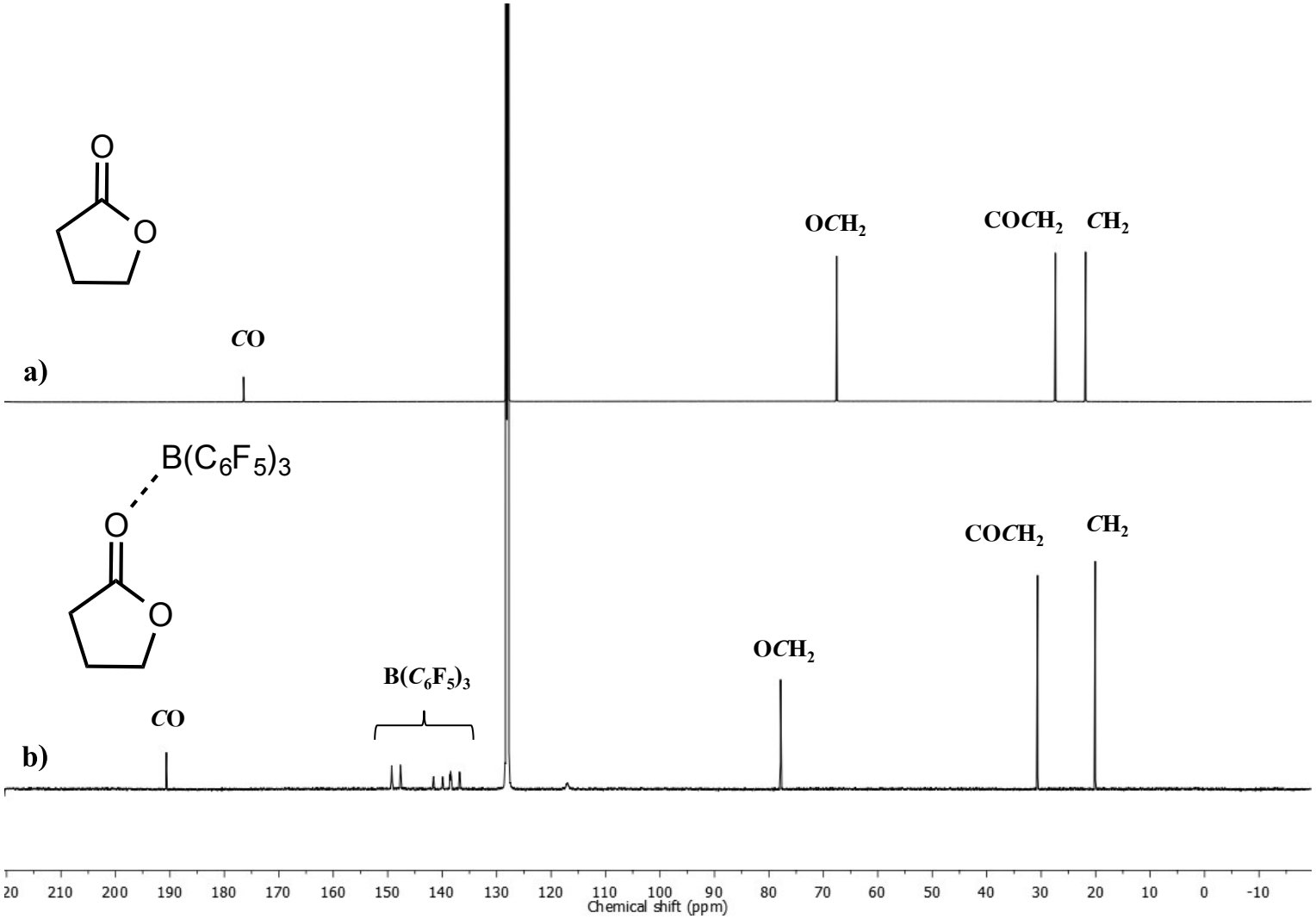

Figure S13 $^{13}C\{^{1}H\}$ NMR spectra (150 MHz, C_6D_6, 30 °C) of a) GBL monomer and b) $B(C_6F_5)_3$·GBL adduct.

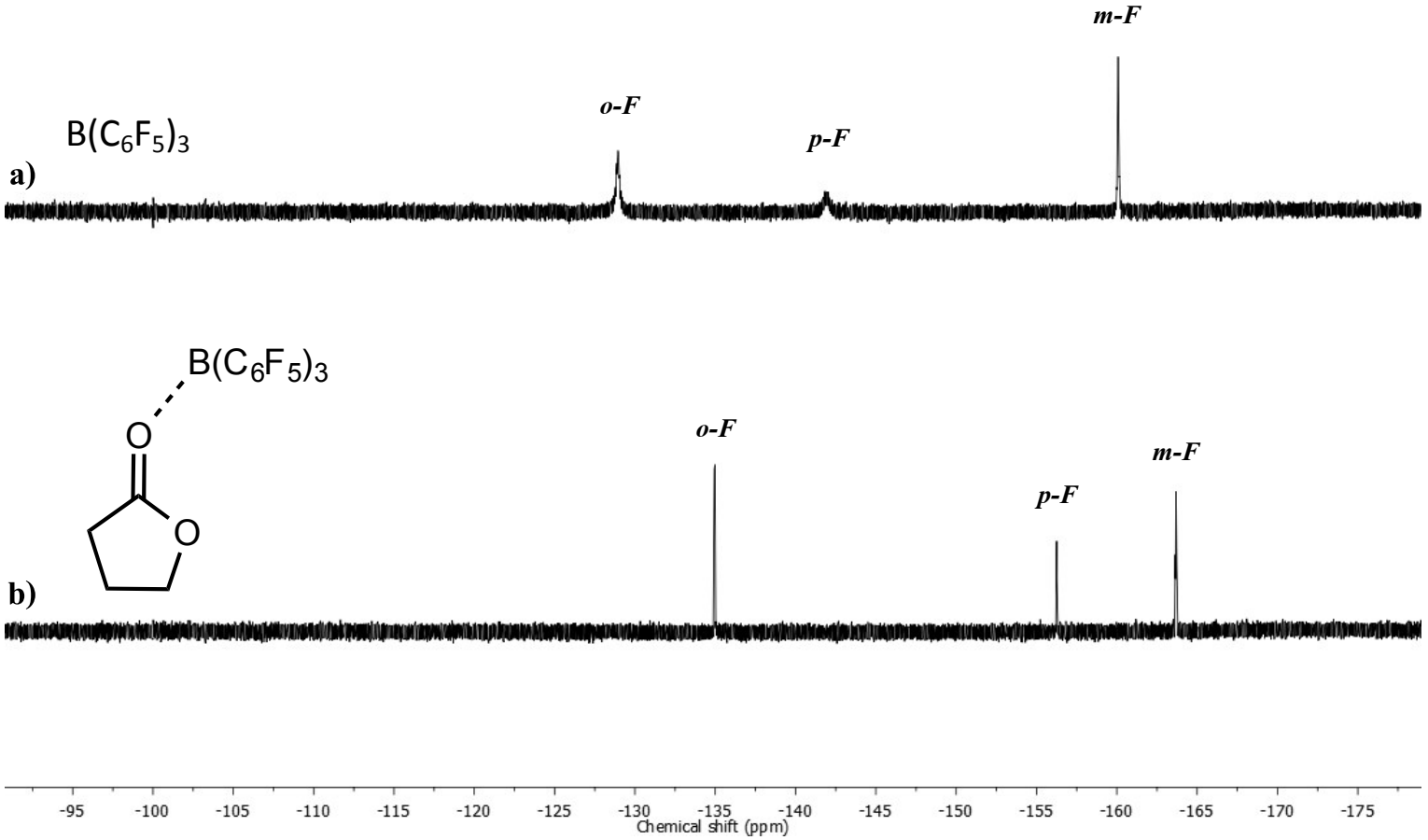

Figure S14 $^{19}F\{^{1}H\}$ NMR spectra (565 MHz, C_6D_6, 30 °C) of a) $B(C_6F_5)_3$ and b) $B(C_6F_5)_3$·GBL adduct.

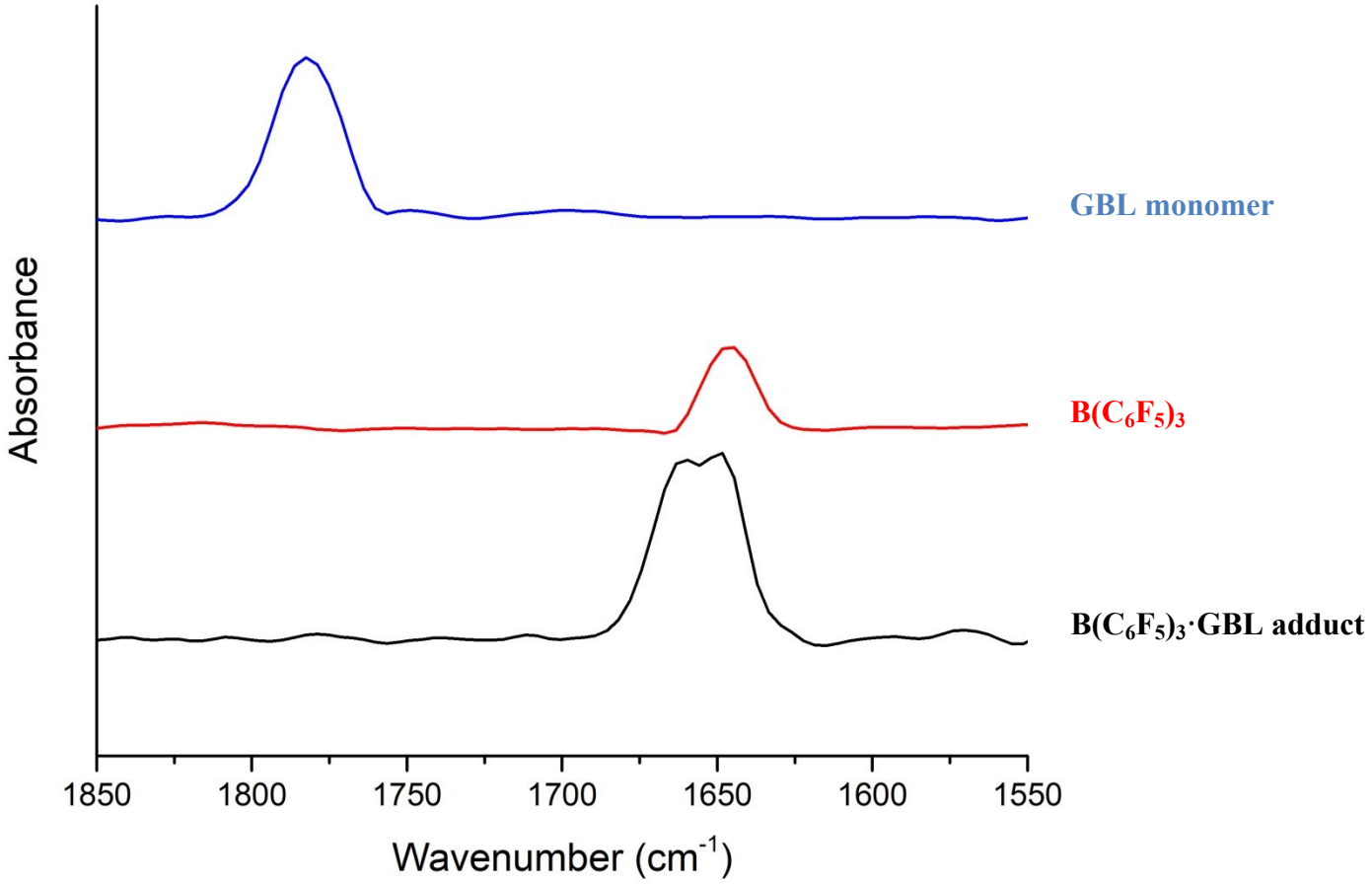

Figure S15 Selected IR spectra of $B(C_6F_5)_3$·GBL adduct (black line), $B(C_6F_5)_3$ (red line), and GBL monomer (blue line) in the region of 1850 – 1550 cm^{-1}. The relative intensities are normalized and thus are directly comparable.

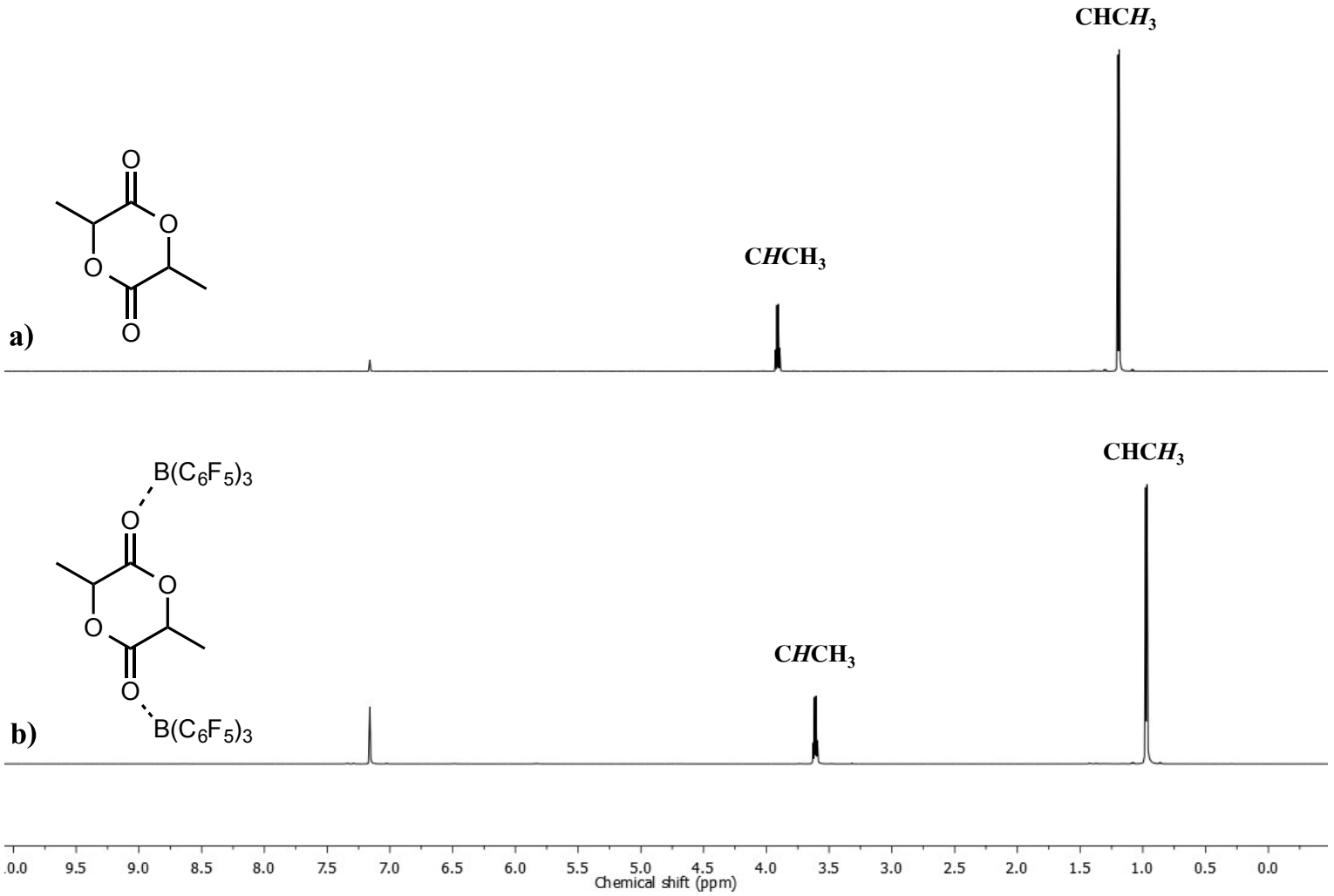

Figure S16 ^{1}H NMR spectra (600 MHz, C_6D_6, 30 °C) of a) LA monomer and b) $B(C_6F_5)_3$·LA adduct.

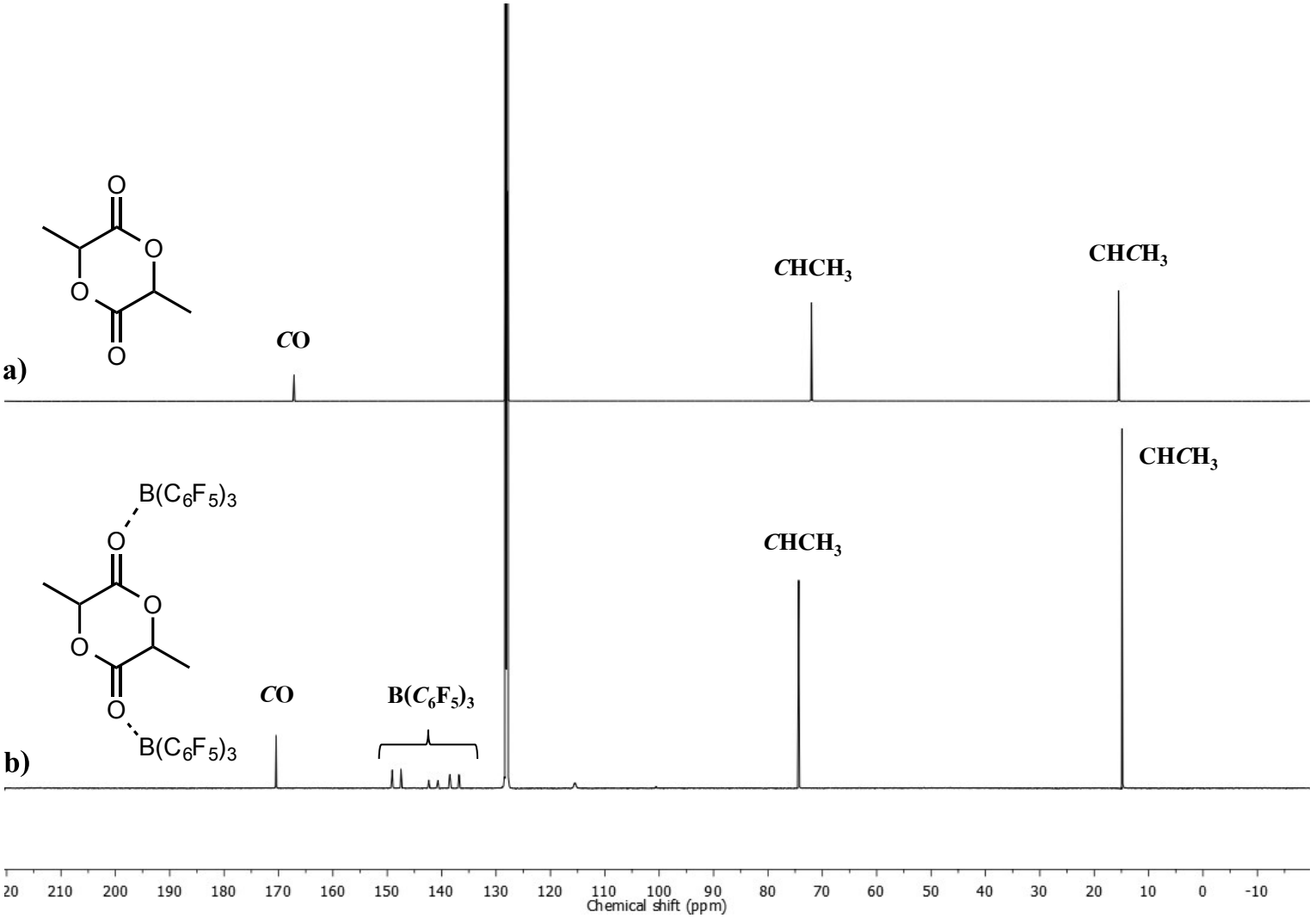

Figure S17 $^{13}C\{^{1}H\}$ NMR spectra (150 MHz, C_6D_6, 30 °C) of a) LA monomer and b) $B(C_6F_5)_3$·LA adduct.

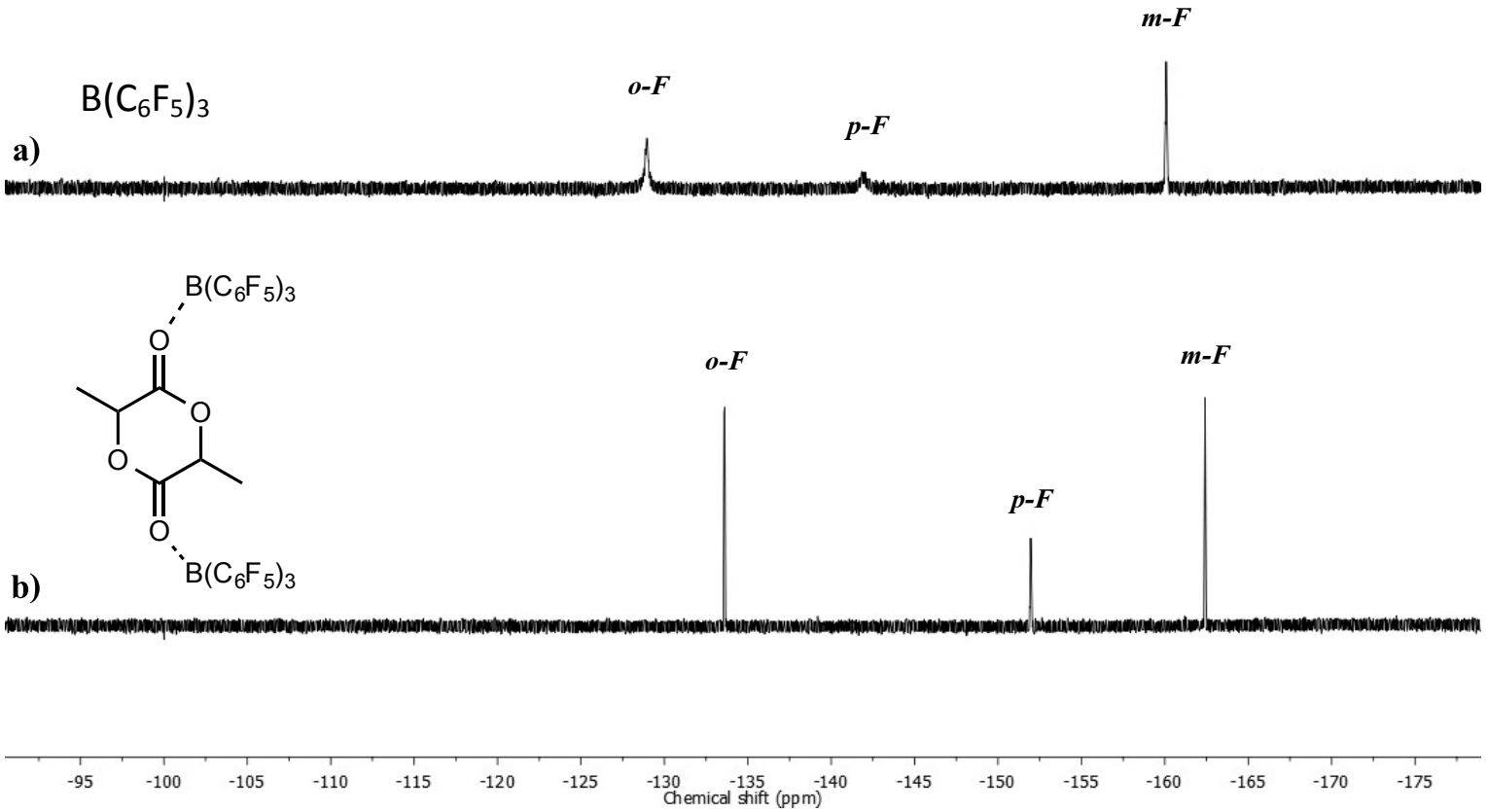

Figure S18 $^{19}F\{^{1}H\}$ NMR spectra (565 MHz, C_6D_6, 30 °C) of a) $B(C_6F_5)_3$ and b) $B(C_6F_5)_3$·LA adduct.

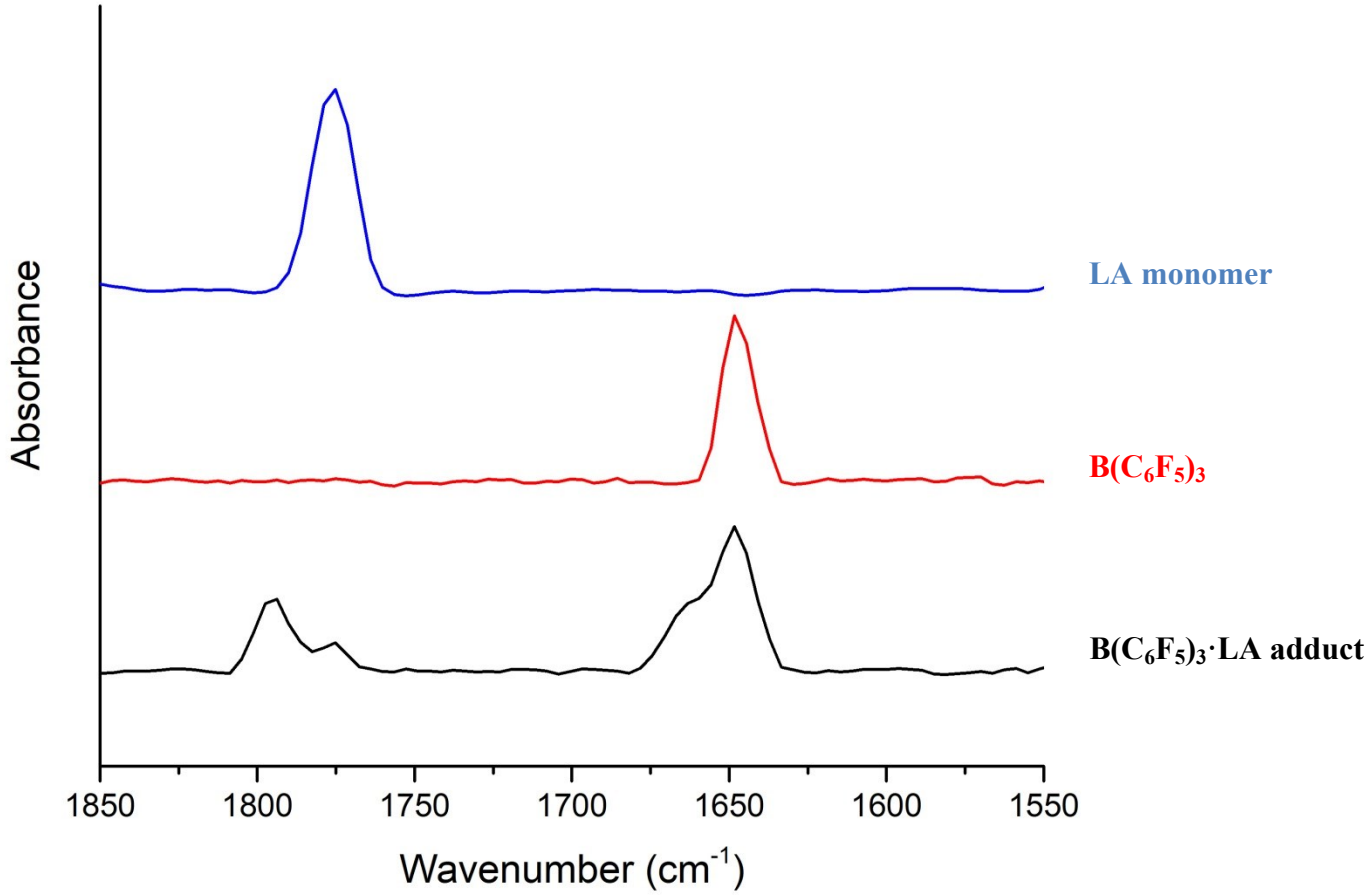

Figure S19 Selected IR spectra of $B(C_6F_5)_3$·LA adduct (black line), $B(C_6F_5)_3$ (red line), and LA monomer (blue line) in the region of 1850 – 1550 cm^{-1}. The relative intensities are normalized and thus are directly comparable.

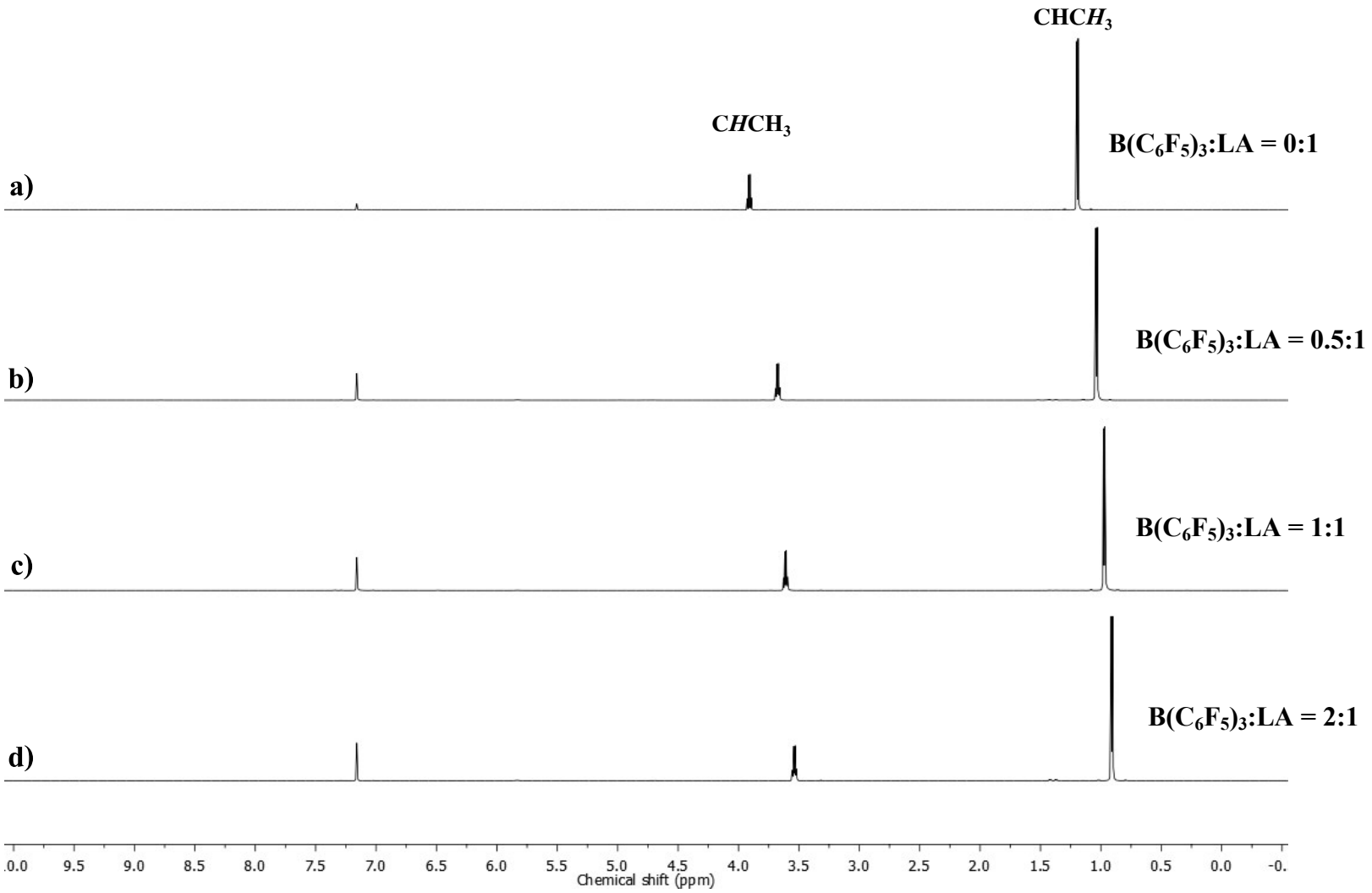

Figure S20 ^{1}H NMR spectra (600 MHz, C_6D_6, 30 °C) of a mixture of $B(C_6F_5)_3$ and LA in the $B(C_6F_5)_3$: LA ratios of a) 0:1, b) 0.5:1, c) 1:1, and d) 2:1.

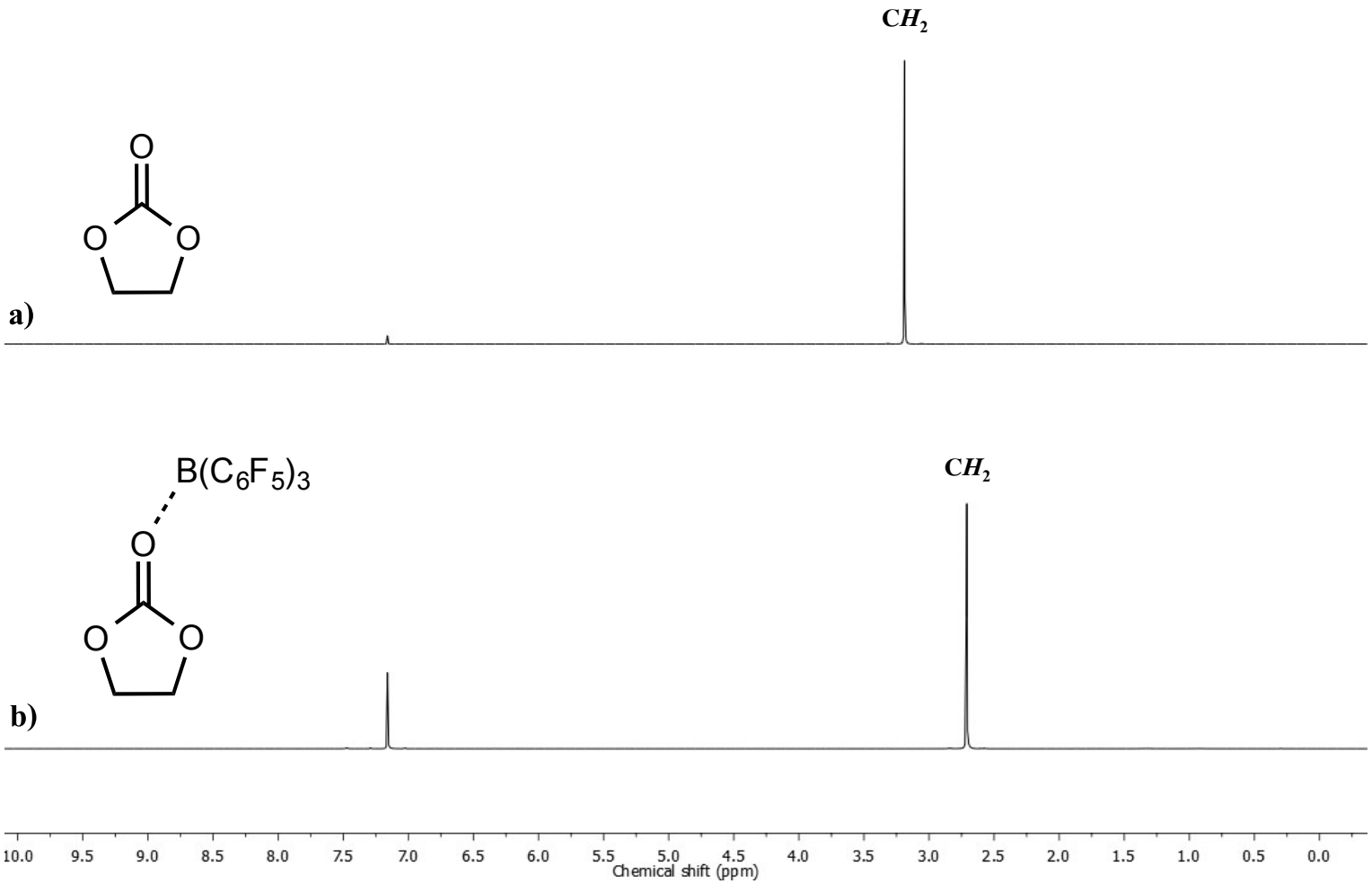

Figure S21 ^{1}H NMR spectra (600 MHz, C_6D_6, 30 °C) of a) EC monomer and b) $B(C_6F_5)_3$·EC adduct.

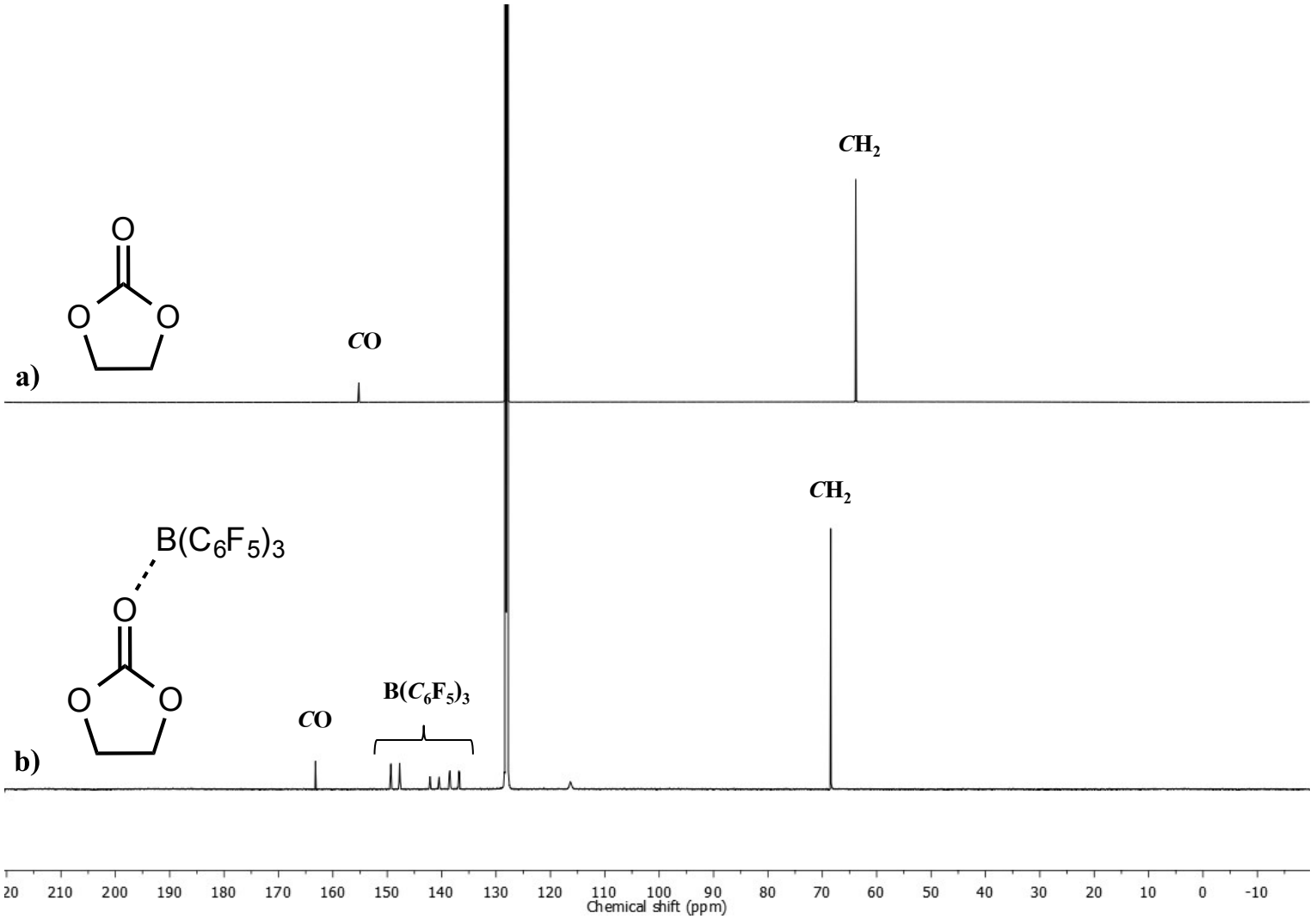

Figure S22 $^{13}C\{^{1}H\}$ NMR spectra (150 MHz, C_6D_6, 30 °C) of a) EC monomer and b) $B(C_6F_5)_3 \cdot$EC adduct.

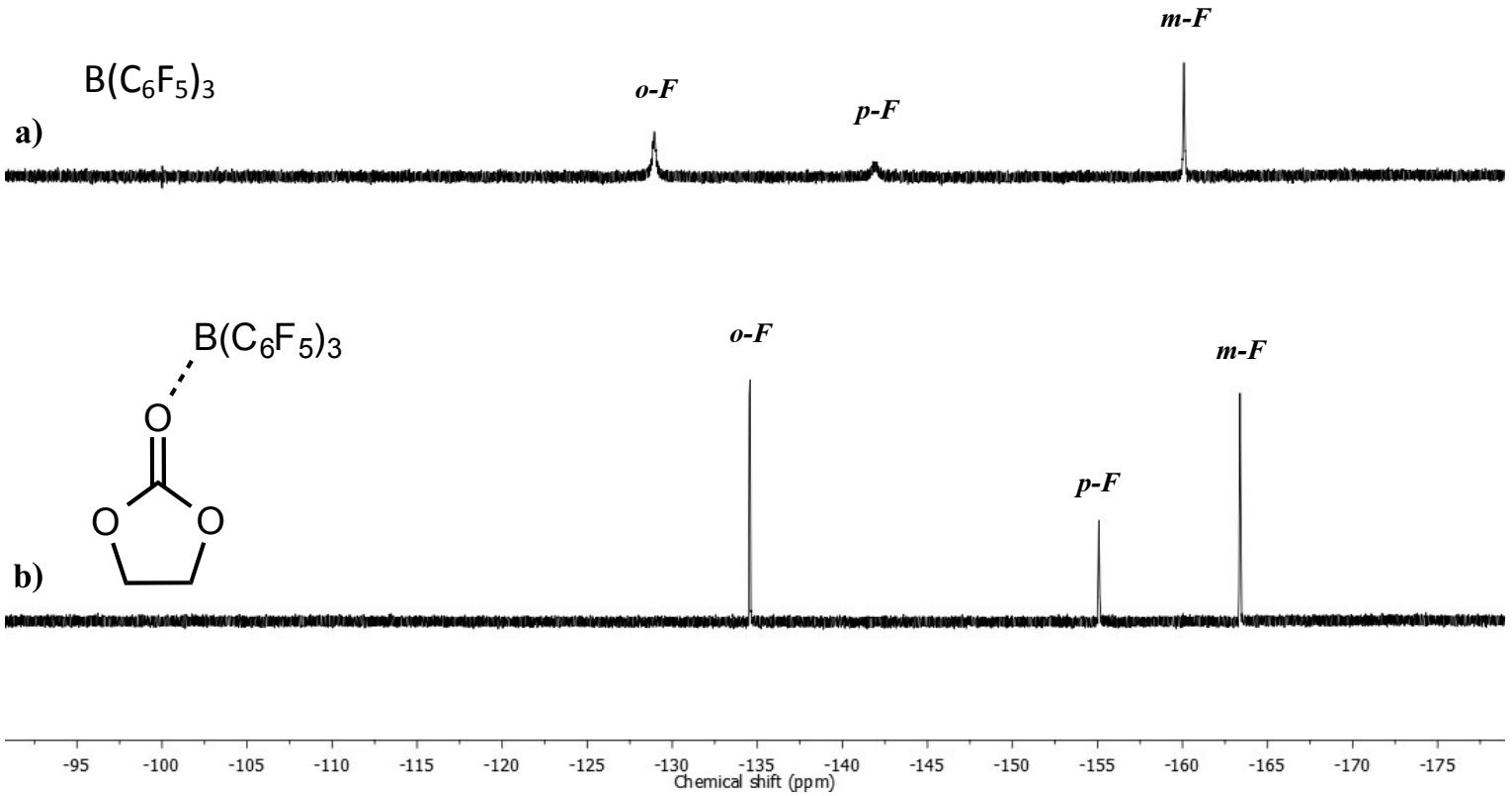

Figure S23 $^{19}F\{^{1}H\}$ NMR spectra (565 MHz, C_6D_6, 30 °C) of a) $B(C_6F_5)_3$ and b) $B(C_6F_5)_3$·EC adduct.

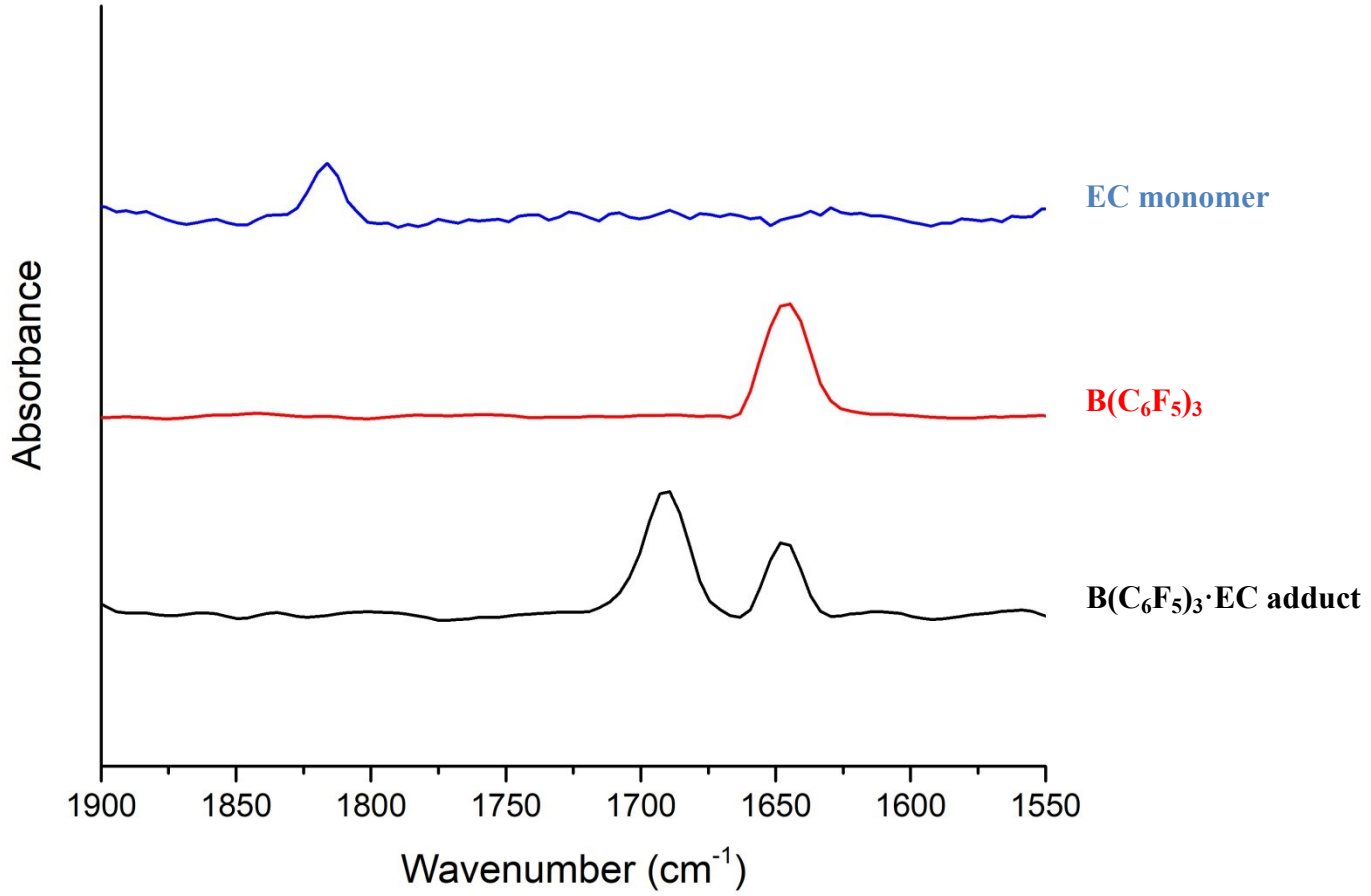

Figure S24 Selected IR spectra of $B(C_6F_5)_3$·EC adduct (black line), $B(C_6F_5)_3$ (red line), and EC monomer (blue line) in the region of 1900 – 1550 cm^{-1}. The relative intensities are normalized and thus are directly comparable.

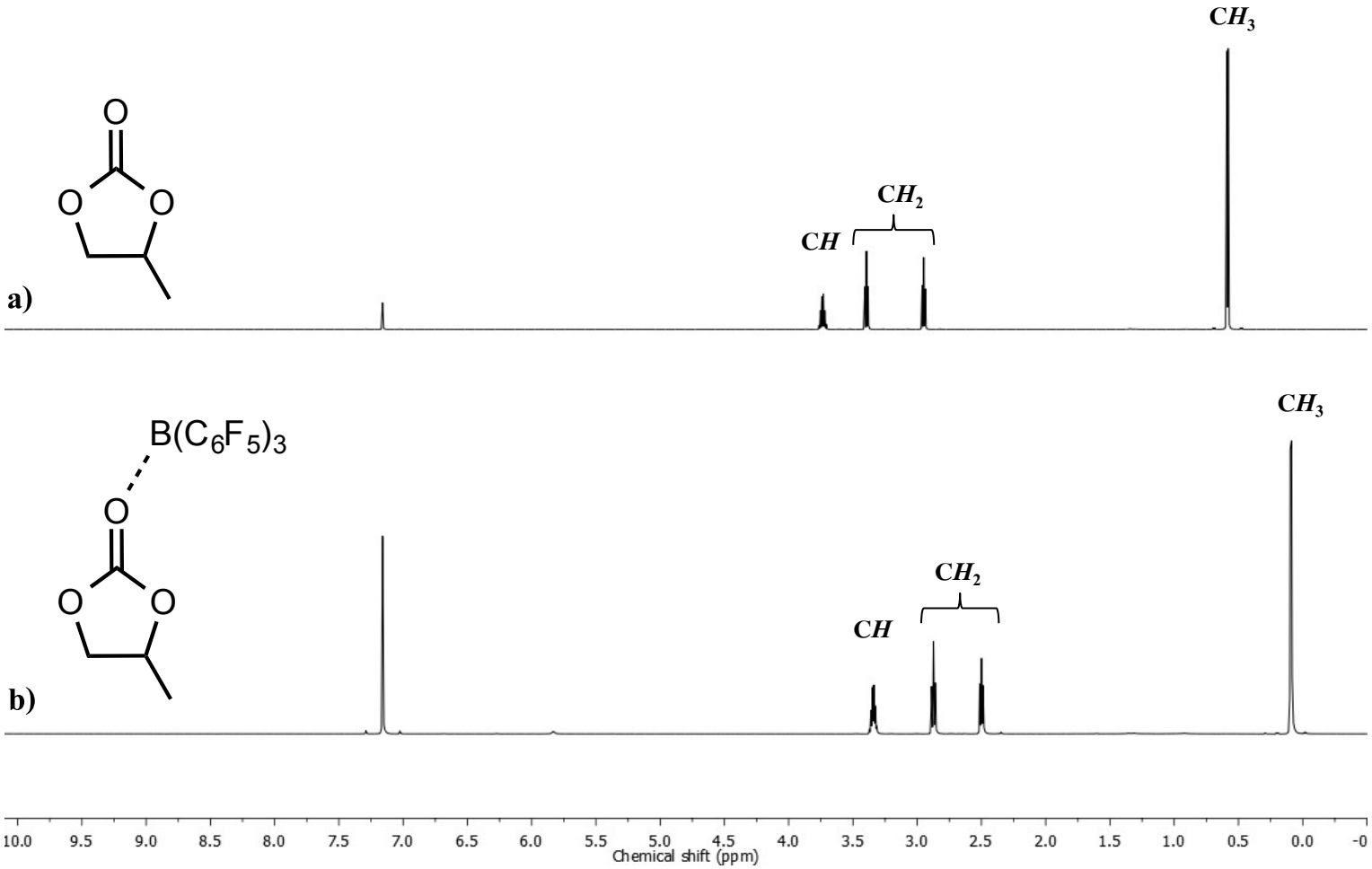

Figure S25 ^{1}H NMR spectra (600 MHz, C_6D_6, 30 °C) of a) PC monomer and b) $B(C_6F_5)_3$·PC adduct.

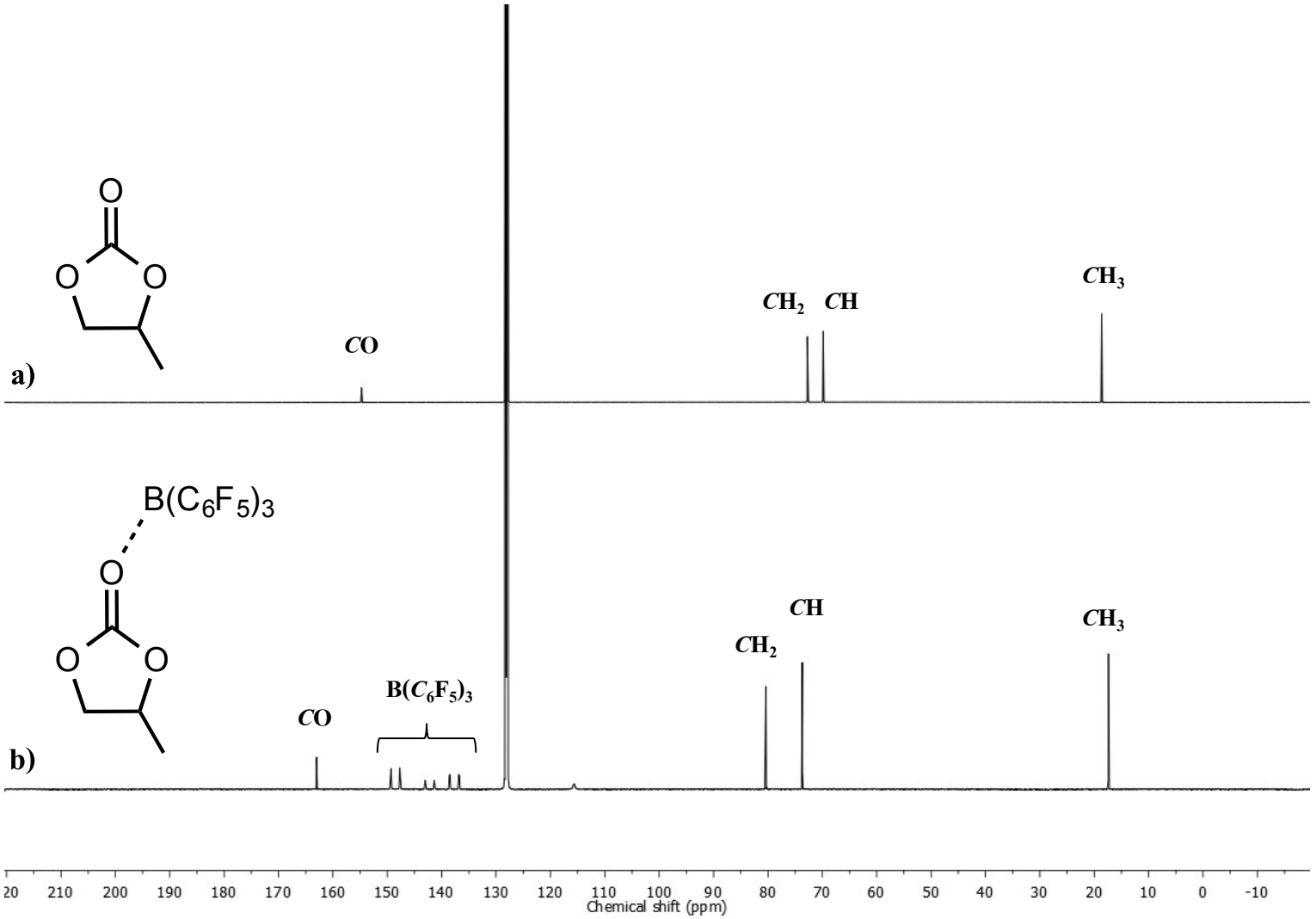

Figure S26 $^{13}C\{^{1}H\}$ NMR spectra (150 MHz, C_6D_6, 30 °C) of a) PC monomer and b) $B(C_6F_5)_3$·PC adduct.

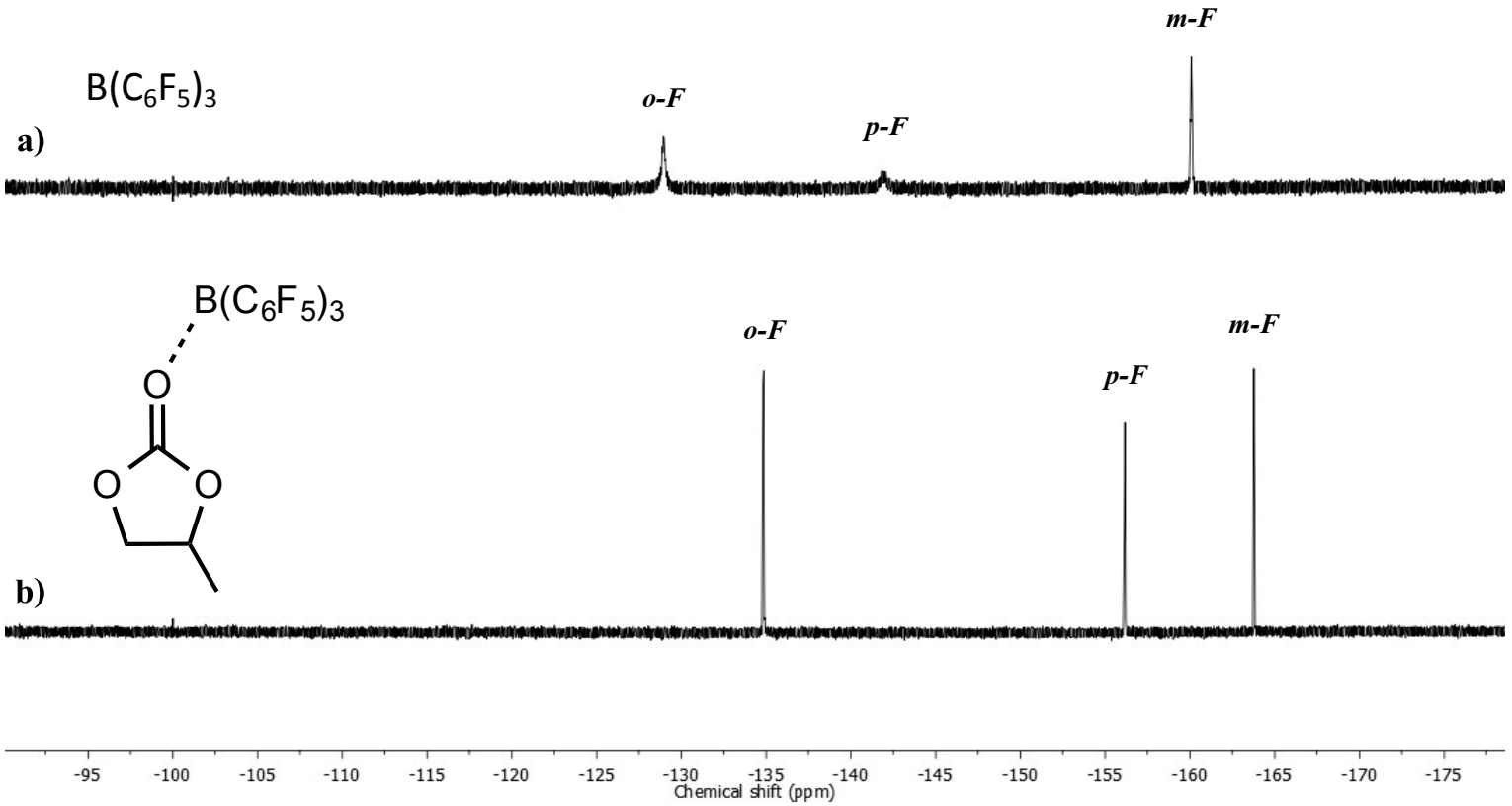

Figure S27 $^{19}F\{^{1}H\}$ NMR spectra (565 MHz, C_6D_6, 30 °C) of a) $B(C_6F_5)_3$ and b) $B(C_6F_5)_3$·PC adduct.

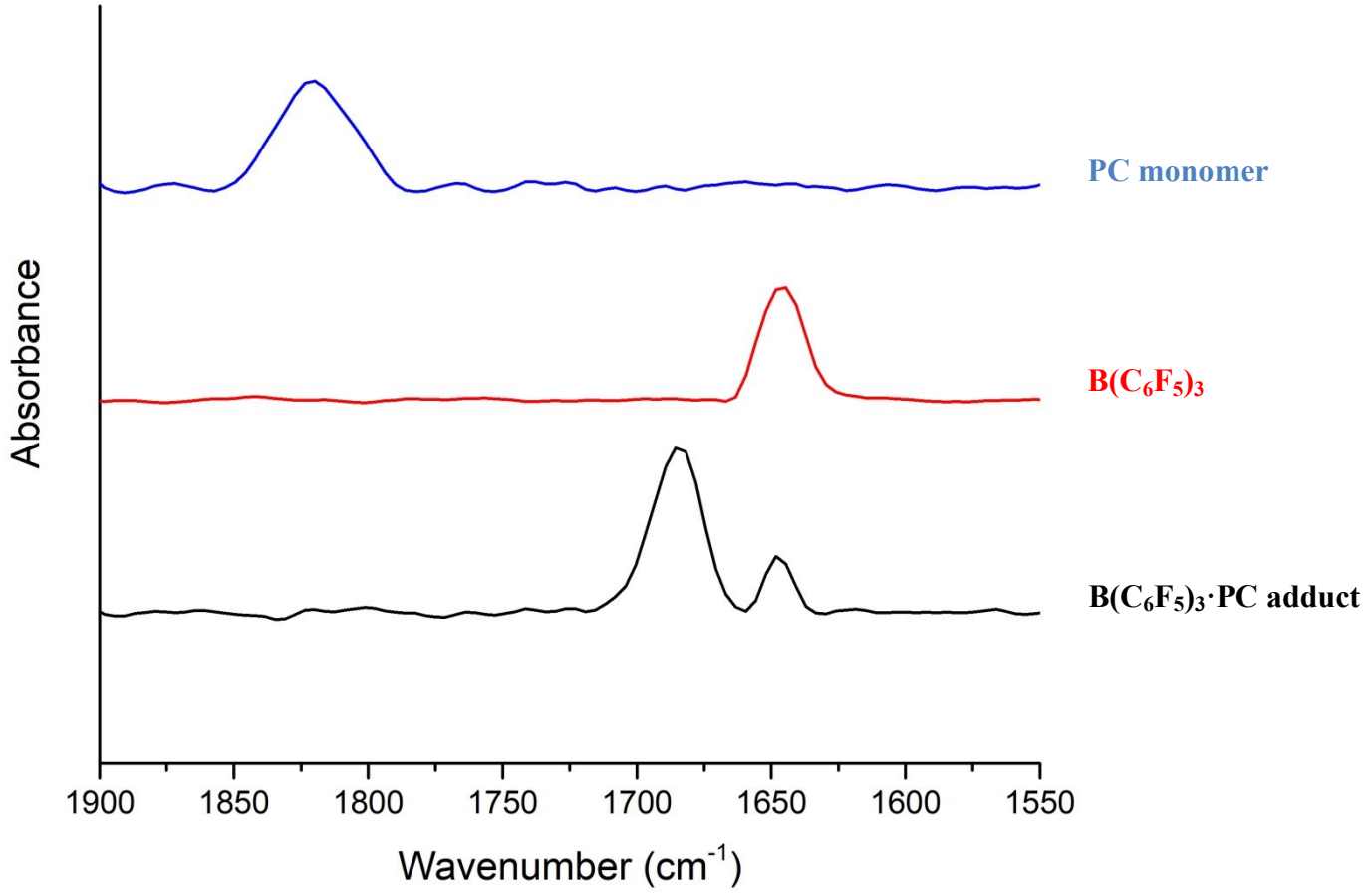

Figure S28 Selected IR spectra of $B(C_6F_5)_3$·PC adduct (black line), $B(C_6F_5)_3$ (red line), and PC monomer (blue line) in the region of 1900 – 1550 cm^{-1}. The relative intensities are normalized and thus are directly comparable.

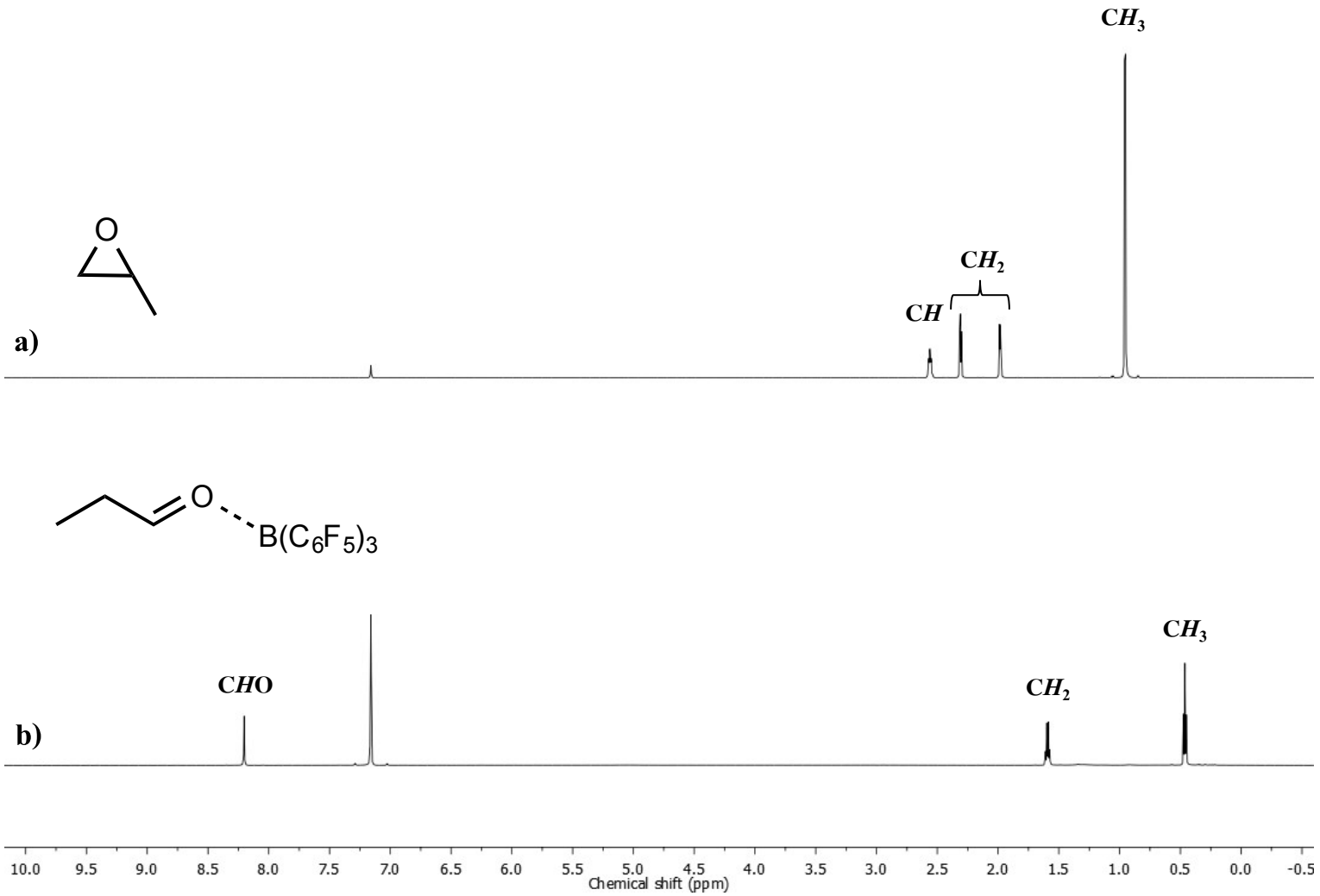

Figure S29 ^{1}H NMR spectra (600 MHz, C_6D_6, 30 °C) of a) PO monomer and b) $CH_3CH_2CHO{\cdot}B(C_6F_5)_3$ adduct.

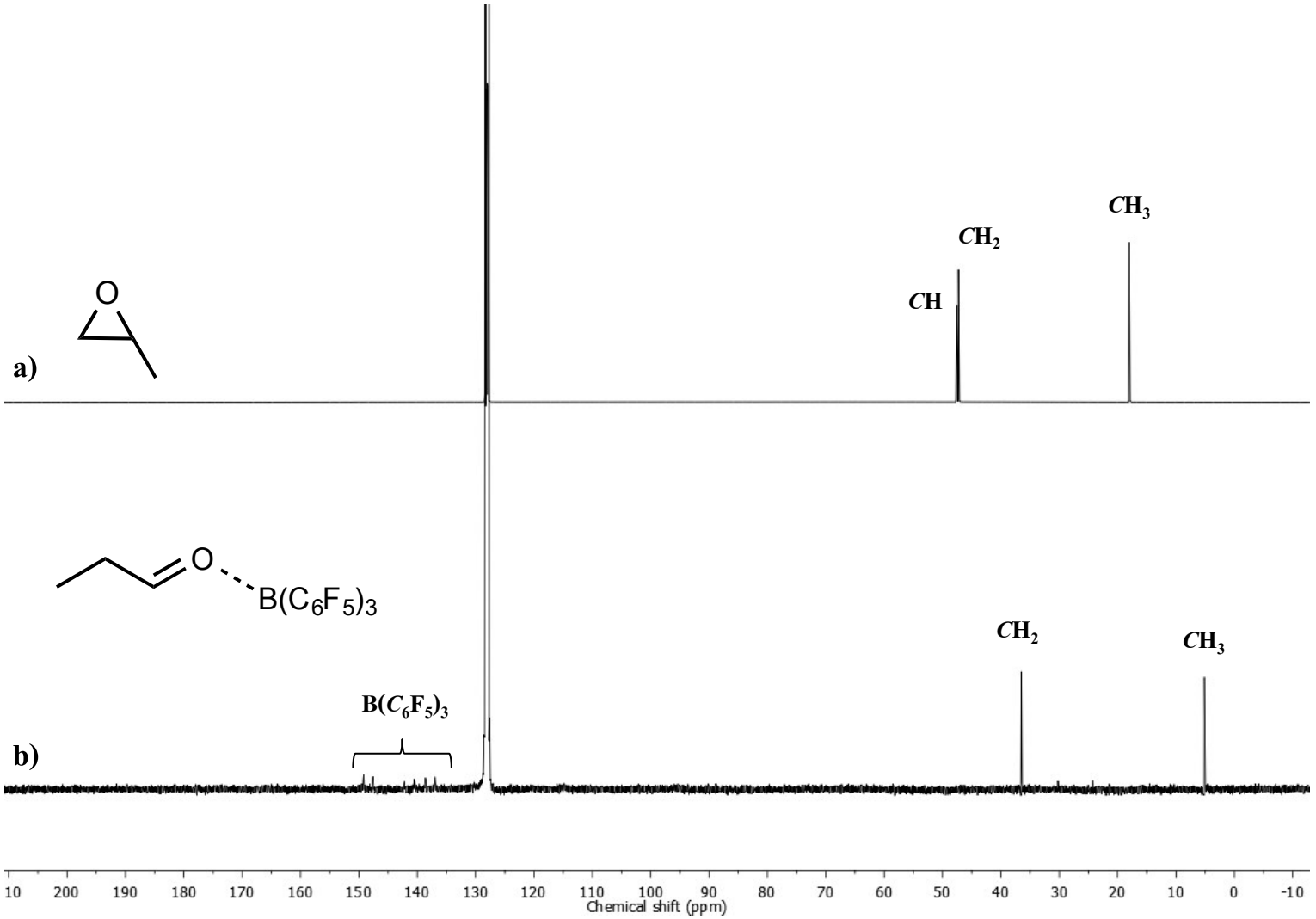

Figure S30 $^{13}C\{^{1}H\}$ NMR spectra (150 MHz, C_6D_6, 30 °C) of a) PO monomer and b) $CH_3CH_2CHO{\cdot}B(C_6F_5)_3$ adduct.

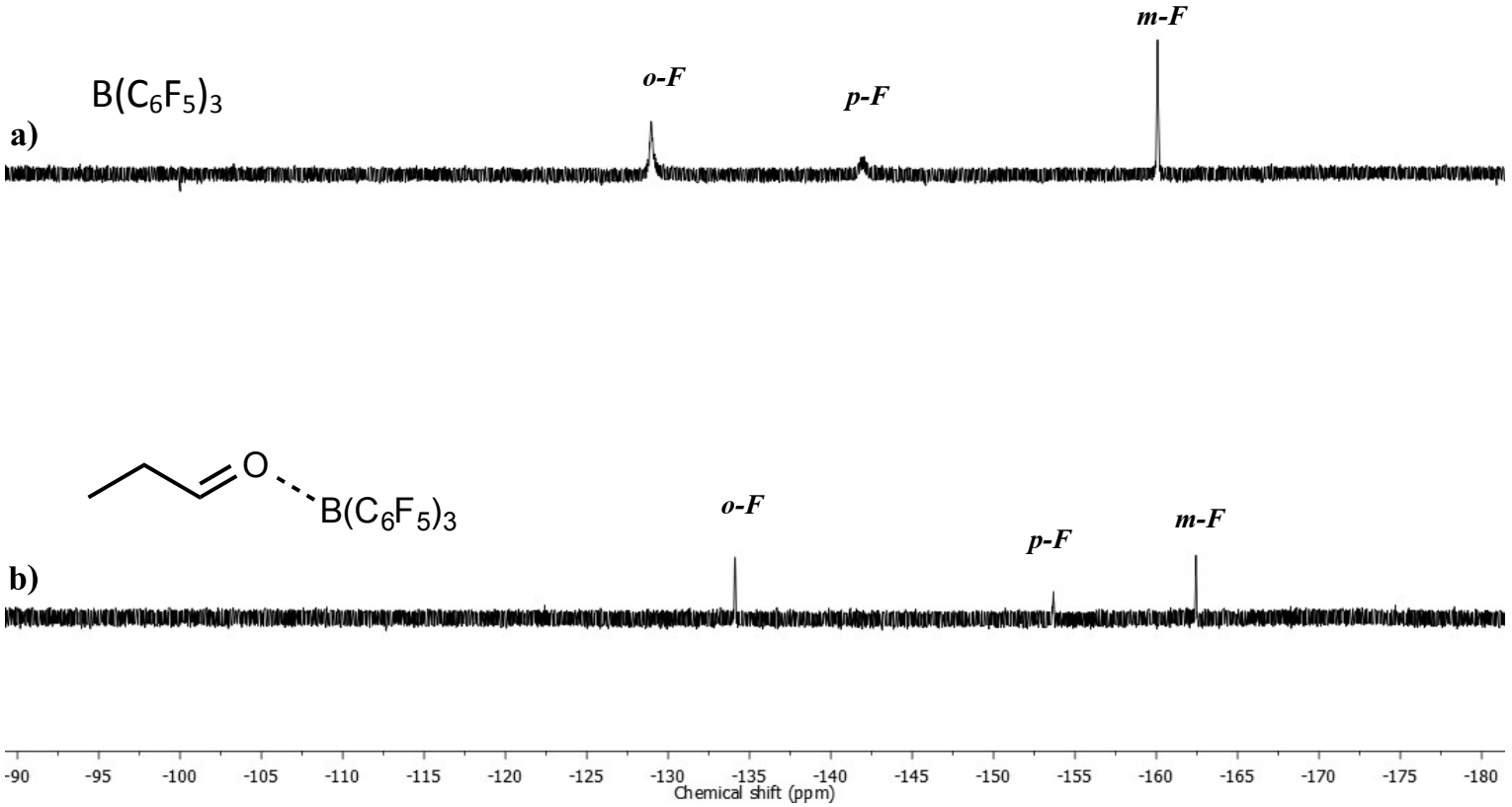

Figure S31 $^{19}F\{^{1}H\}$ NMR spectra (565 MHz, C_6D_6, 30 °C) of a) $B(C_6F_5)_3$ and b) $CH_3CH_2CHO{\cdot}B(C_6F_5)_3$ adduct.

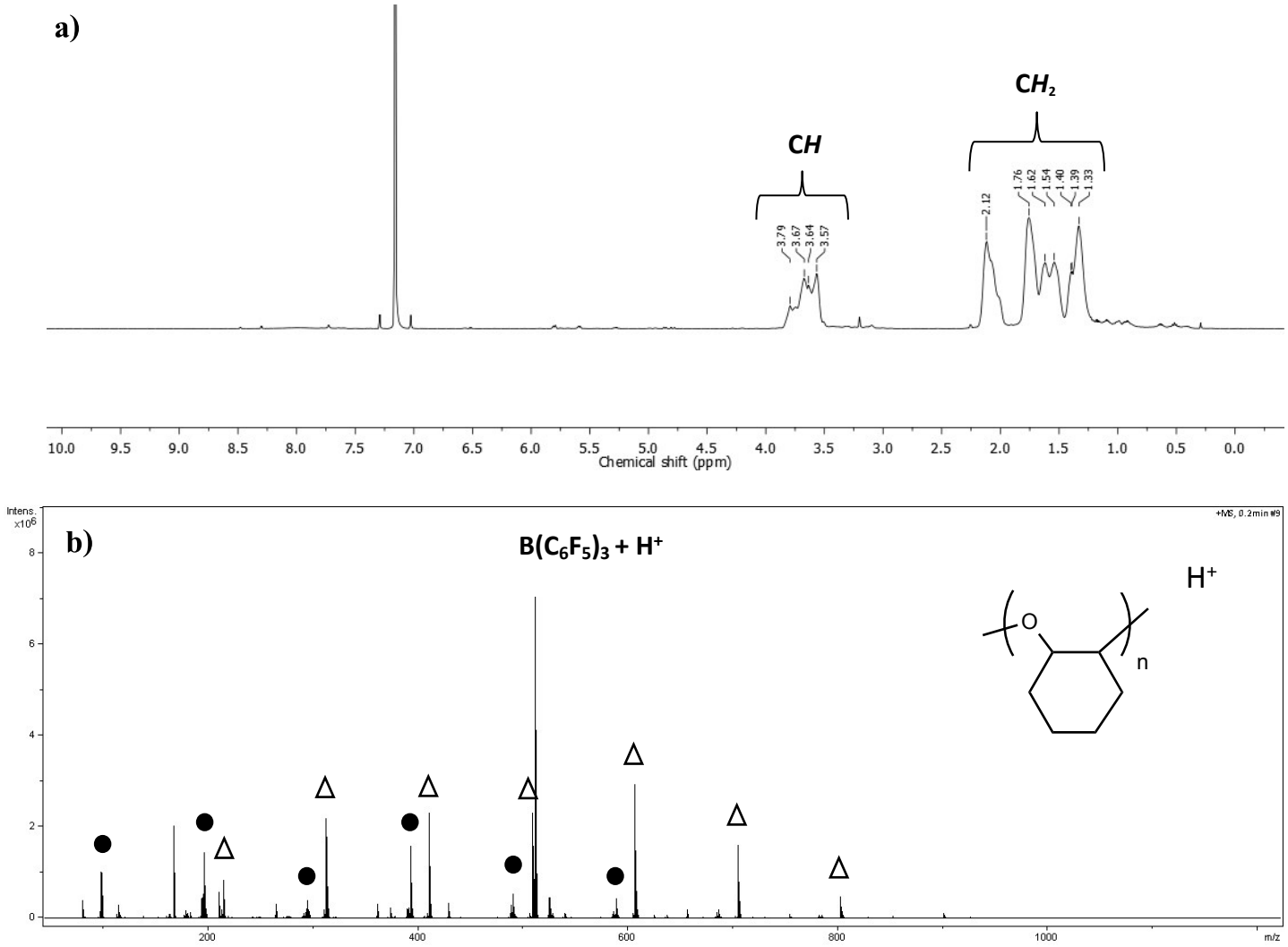

Figure S32 a) ^{1}H NMR spectra (600 MHz, C_6D_6, 30 °C) of oligo(cyclohexene oxide) and b) APCI mass spectrum of oligo(cyclohexene oxide): ● = $(CHO)_n + H^+$; Δ = $H\text{-}(CHO)_n\text{-}OH + H^+$.

5. Competitive Coordination Studies

- **Comparison between CL and PC.**

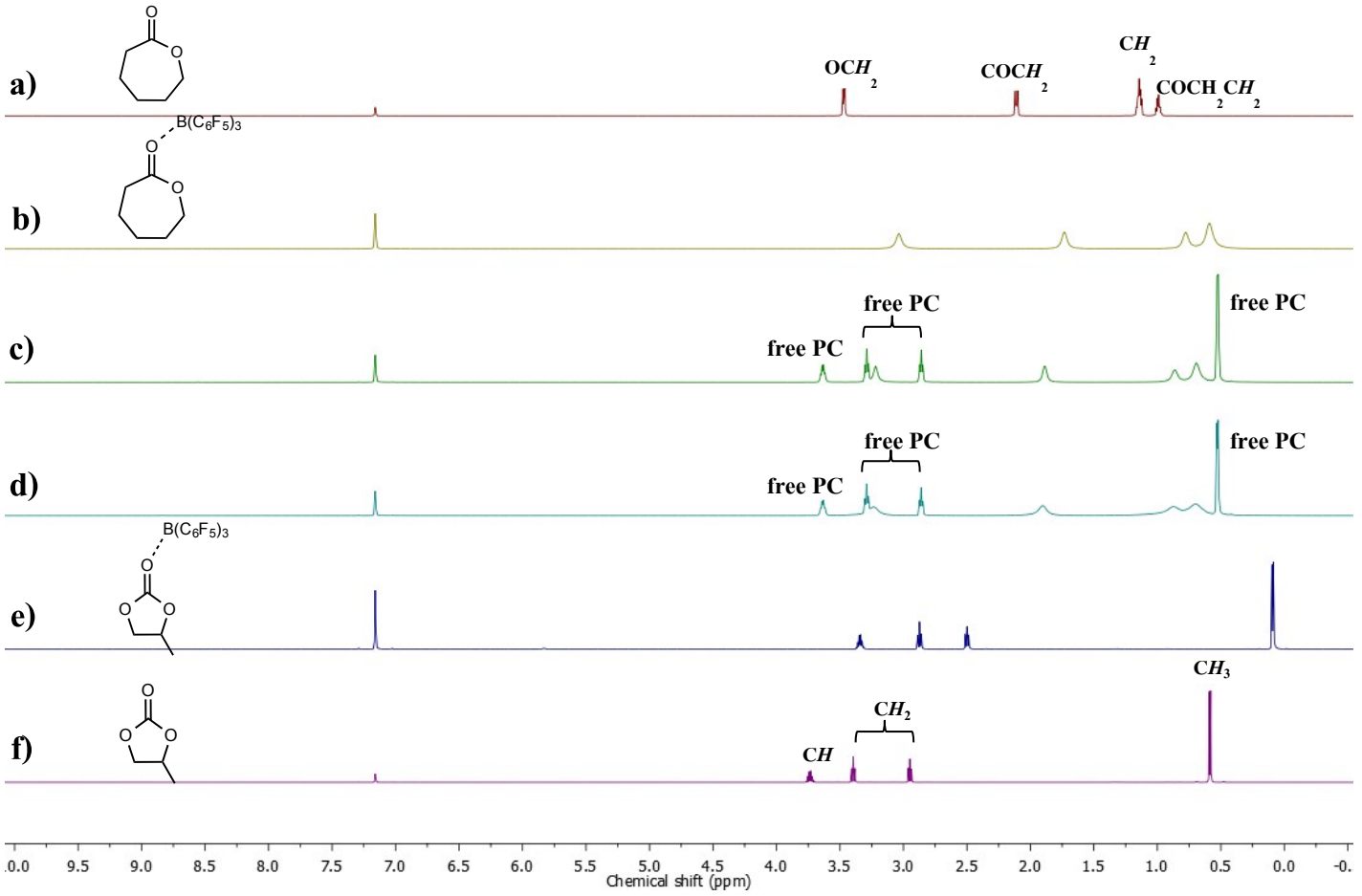

Figure S33 ^{1}H NMR spectra (600 MHz, C_6D_6, 30 °C) of a) CL monomer, b) $B(C_6F_5)_3$·CL adduct, c) adding PC to $B(C_6F_5)_3$·CL adduct, d) adding CL to $B(C_6F_5)_3$·PC adduct, e) $B(C_6F_5)_3$·PC adduct, and f) PC monomer.

➢ **Comparison between CL and THF.**

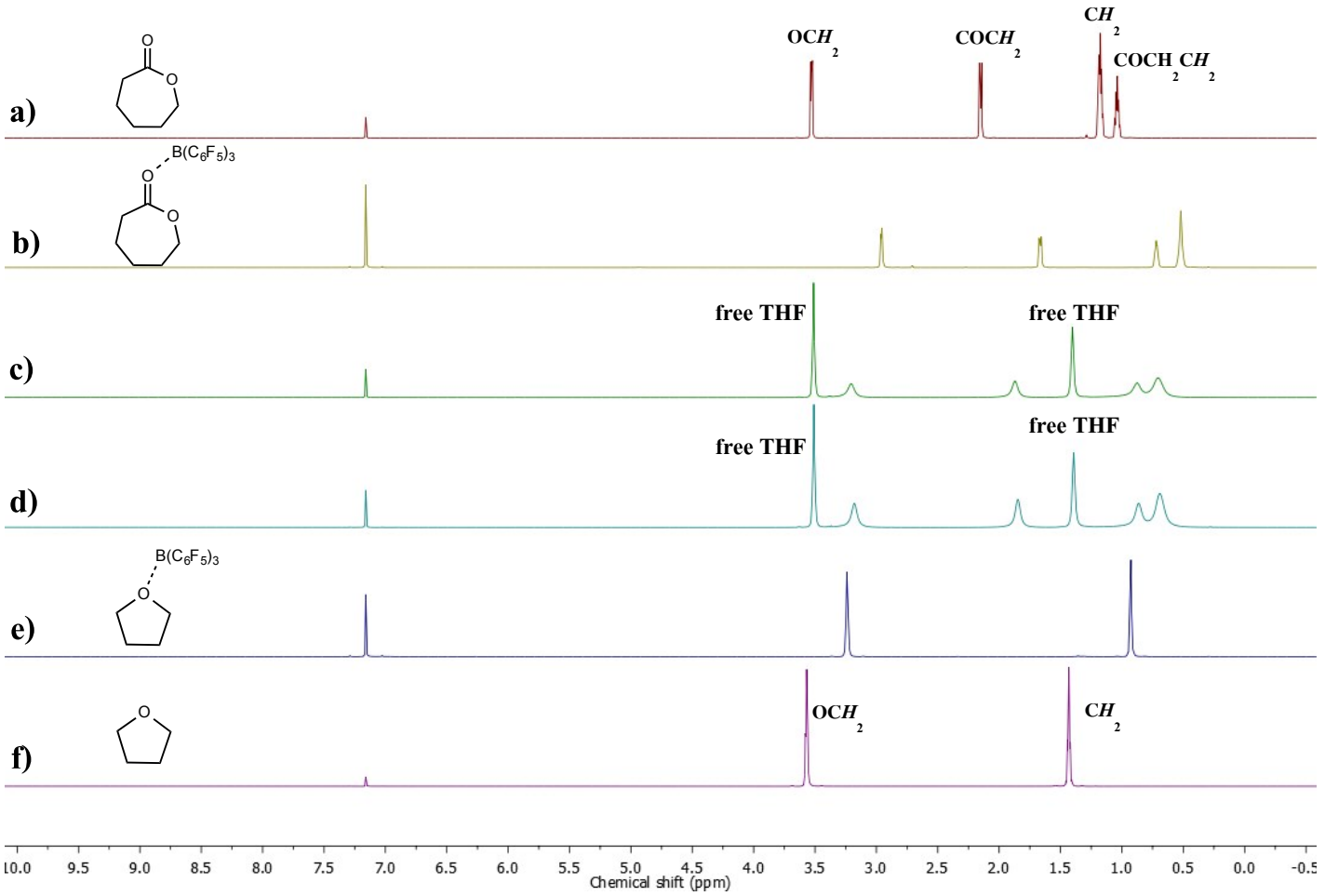

Figure S34 ^{1}H NMR spectra (600 MHz, C_6D_6, 30 °C) of a) CL monomer, b) $B(C_6F_5)_3$·CL adduct, c) adding THF to $B(C_6F_5)_3$·CL adduct, d) adding CL to $B(C_6F_5)_3$·THF adduct, e) $B(C_6F_5)_3$·THF adduct, and f) THF.

➢ **Comparison between LA and PC.**

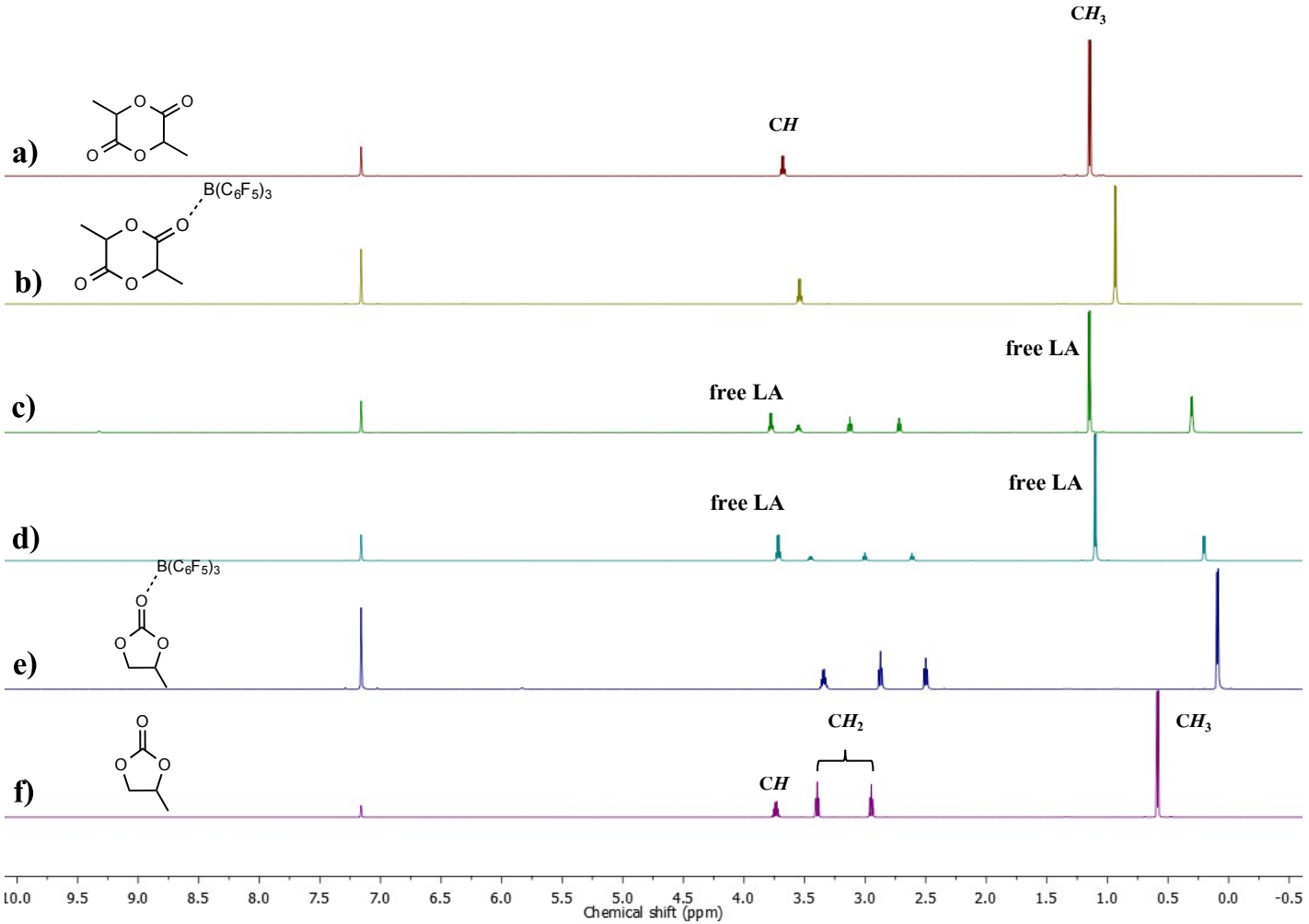

Figure S35 ^{1}H NMR spectra (600 MHz, C_6D_6, 30 °C) of a) LA monomer, b) $B(C_6F_5)_3$·LA adduct, c) adding PC to $B(C_6F_5)_3$·LA adduct, d) adding LA to $B(C_6F_5)_3$·PC adduct, e) $B(C_6F_5)_3$·PC adduct, and f) PC monomer.

➢ **Comparison between LA and THF.**

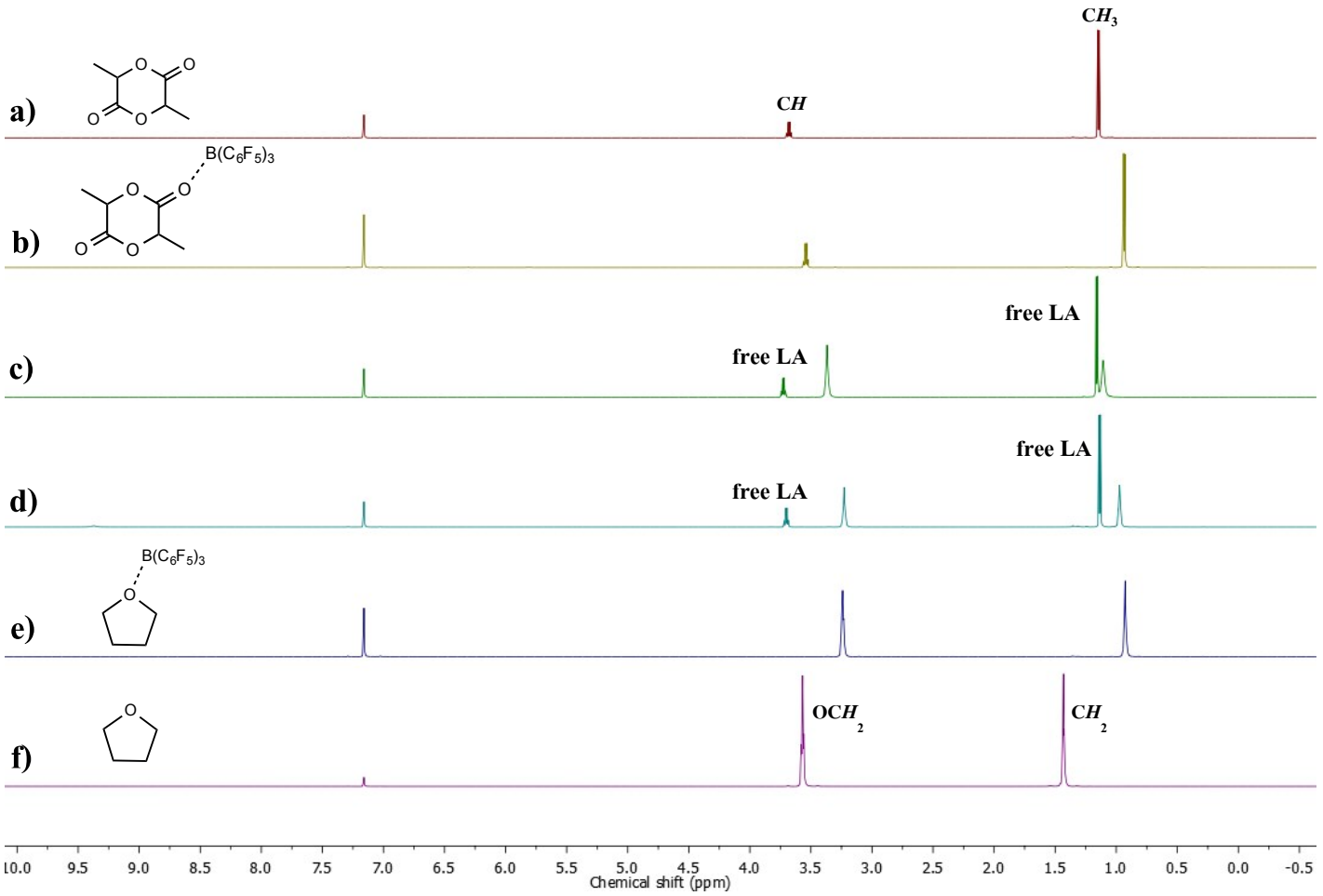

Figure S36 ^{1}H NMR spectra (600 MHz, C_6D_6, 30 °C) of a) LA monomer, b) $B(C_6F_5)_3$·LA adduct, c) adding THF to $B(C_6F_5)_3$·LA adduct, d) adding LA to $B(C_6F_5)_3$·THF adduct, e) $B(C_6F_5)_3$·THF adduct, and f) THF.

➢ **Comparison between PC and THF.**

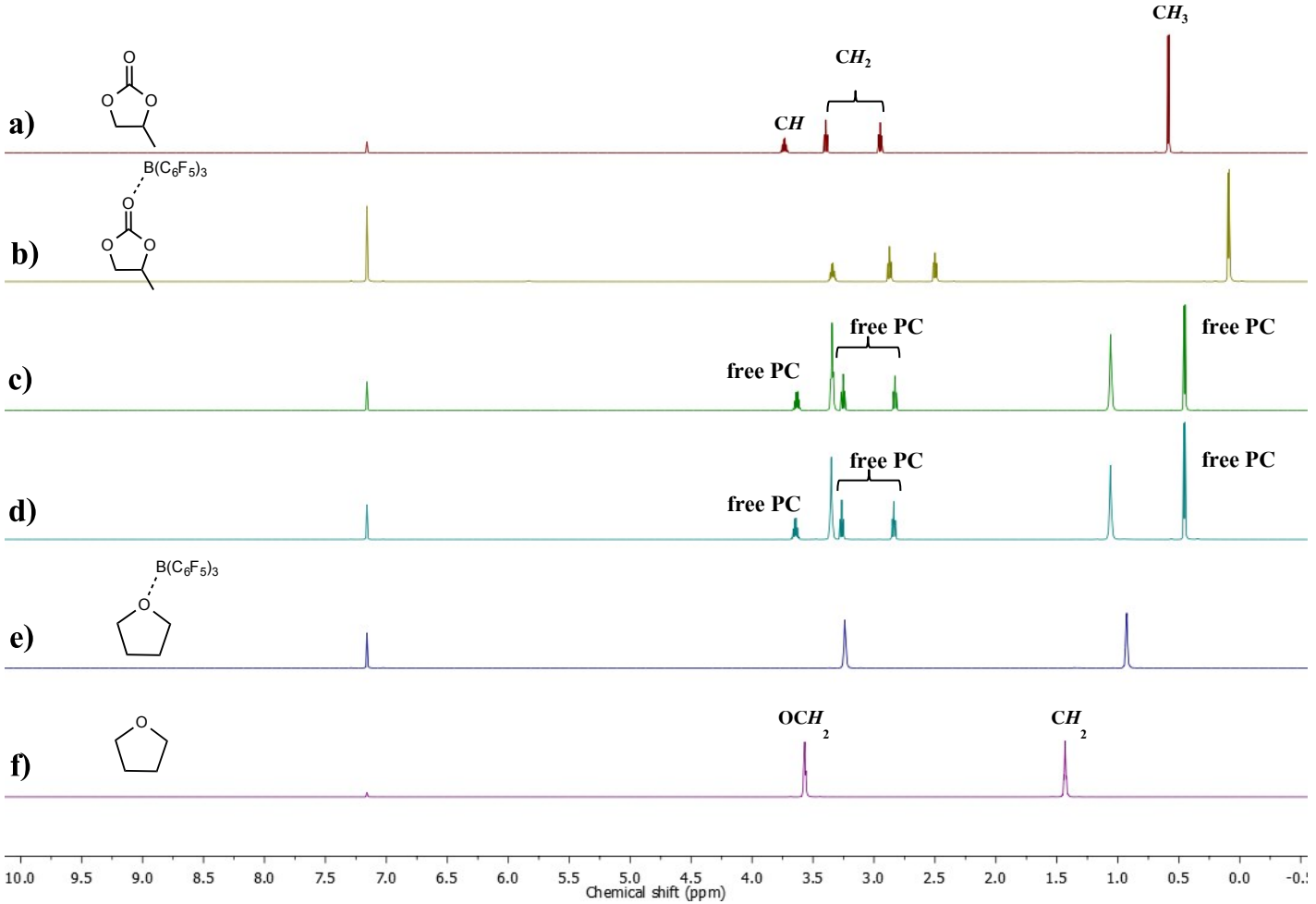

Figure S37 ^{1}H NMR spectra (600 MHz, C_6D_6, 30 °C) of a) PC monomer, b) $B(C_6F_5)_3$·PC adduct, c) adding THF to $B(C_6F_5)_3$·PC adduct, d) adding PC to $B(C_6F_5)_3$·THF adduct, e) $B(C_6F_5)_3$·THF adduct, and f) THF.

6. DFT calculations

All calculations were carried out with GAUSSIAN 09 program.[1] The structural optimization was performed using B3LYP[2-3] functional and 6-31G(d,p)[4] basis set. The gas phase optimized geometries of all structures were in good agreement regarding bond lengths and angles of X-ray crystallographic result. Further single point energy calculations and solvent effects in benzene which computed using the polarizable continuum model (PCM) model[5] were performed at B3LYP level with 6-311G(d,p) basis set on B3LYP/6-31G(d,p) geometries.[6]

The free adsorption energy (ΔG) values of each Lewis acid-base adduct were calculated from the coordination of $B(C_6F_5)_3$ and each cyclic monomer at oxygen atom of carbonyl group as shown in Eq. 1.

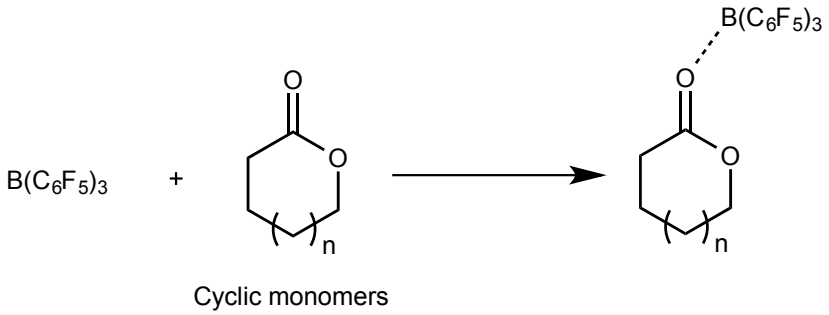

Eq. 1

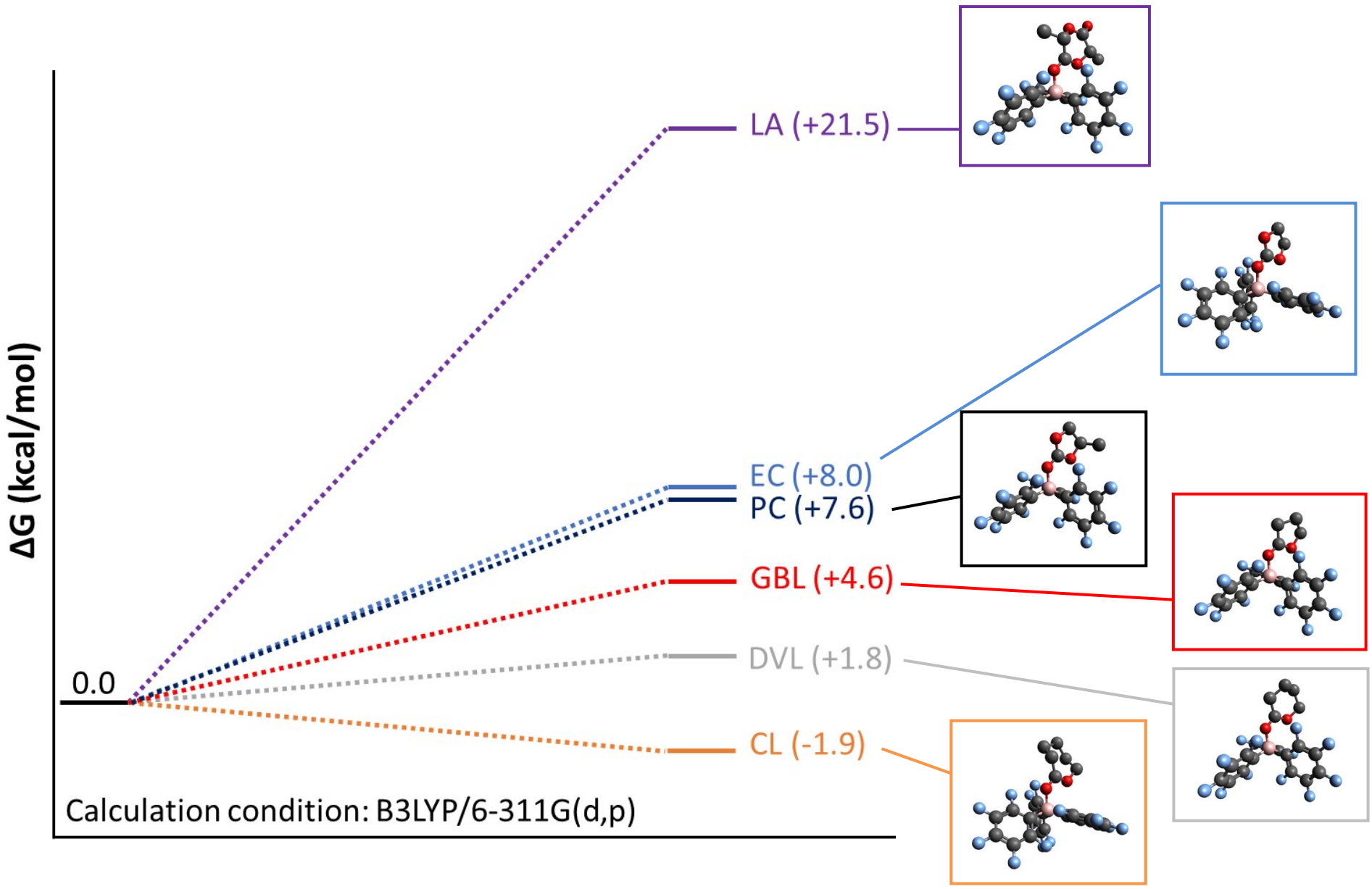

Figure S38 The calculated free adsorption energy of each Lewis acid-base adduct between $B(C_6F_5)_3$ and cyclic monomers.

References (for DFT calculations)

(1) *Gaussian 09, Rev. A.02*, Frisch, M. J.; Trucks, G. W.; Schlegel, H. B.; Scuseria, G. E.; Robb, M. A.; Cheeseman, J. R.; Scalmani, G.; Barone, V.; Petersson, G. A.; Nakatsuji, H.; Li, X.; Caricato, M.; Marenich, A. V.; Bloino, J.; Janesko, B. G.; Gomperts, R.; Mennucci, B.; Hratchian, H. P.; Ortiz, J. V.; Izmaylov, A. F.; Sonnenberg, J. L.; Williams; Ding, F.; Lipparini, F.; Egidi, F.;Goings, J.; Peng, B.; Petrone, A.; Henderson, T.; Ranasinghe, D.; Zakrzewski, V. G.; Gao, J.; Rega, N.; Zheng, G.; Liang, W.; Hada, M.; Ehara, M.; Toyota, K.; Fukuda, R.; Hasegawa, J.; Ishida, M.; Nakajima, T.; Honda, Y.; Kitao, O.; Nakai, H.; Vreven, T.; Throssell, K.; Montgomery Jr., J. A.; Peralta, J. E.; Ogliaro, F.; Bearpark, M. J.; Heyd, J. J.; Brothers, E. N.; Kudin, K. N.; Staroverov, V. N.; Keith, T. A.; Kobayashi, R.; Normand, J.; Raghavachari, K.; Rendell, A. P.; Burant, J. C.; Iyengar, S. S.; Tomasi, J.; Cossi, M.; Millam, J. M.; Klene, M.; Adamo, C.; Cammi, R.; Ochterski, J. W.; Martin, R. L.; Morokuma, K.; Farkas, O.; Foresman, J. B.; Fox, D. J., Wallingford, CT, 2016.

(2) Becke, A.D. Density Functional Thermochemistry. III. The Role of Exact Exchange *J. Chem. Phys.* **1993**, *98*, 5648–5652, DOI: 10.1063/1.464913.

(3) Lee, C.; Yang, W.; Parr, R.G. Development of the Colle-Salvetti Correlation Energy Formula into a Functional of the Electron Density, *Phys. Rev. B* **1988**, *37*, 785–789, DOI: 10.1103/PhysRevB.37.785.

(4) Frisch, M. J.; Pople, J. A.; Binkley, J. S. Self-consistent molecular orbital methods 25. Supplementary functions for Gaussian basis sets *J. Chem. Phys*. **1984**, *80*, 3265–3269, DOI: 10.1063/1.447079.

(5) (a) Barone, V.; Cossi, M. Quantum Calculation of Molecular Energies and Energy Gradients in Solution by a Conductor Solvent Model. *J. Phys. Chem. A* **1998,** *102*, 1995-2001, DOI: 10.1021/jp9716997. (b) Cossi, M.; Rega, N.; Scalmani, G.; Barone, V. Polarizable dielectric model of solvation with inclusion of charge penetration effects. *J. Chem. Phys.* **2001,** *114*, 5961-5701, DOI: 10.1063/1.1354187. (c) Scalmani, G.; Frisch, M. J. Continuous surface charge polarizable continuum models of solvation. I. General formalism. *J. Chem. Phys.* **2010,** *132*, 114110, DOI: 10.1063/1.3359469.

(6) Rajeshwari, B.; Kalaiselvan, A.; Senthilnathan D. Ab initio and DFT Investigations on the Ring Opening of Aziridines Using Singlet Unsaturated Carbenes. *Comput. Theor. Chem.* **2018**, *1126*, 1–6, DOI: 10.1016/j.comptc.2018.01.012.